
POSTPRINT VERSION

**Small-scale pottery production and distribution in
the southern confines of the Inca Empire: an
archaeometric insight to define the Provincial
style**

Ots, M.J., Buxeda i Garrigós, J., Madrid i Fernández, M., Cahiza, P.A.

To cite this article: Ots, M.J., Buxeda i Garrigós, J., Madrid i Fernández, M. et al. Small-scale pottery production and distribution in the southern confines of the Inca Empire: an archaeometric insight to define the Provincial style. *Archaeol Anthropol Sci* 16, 37 (2024). <https://doi.org/10.1007/s12520-024-01934-5>

To link to this article: <https://doi.org/10.1007/s12520-024-01934-5>

SMALL-SCALE POTTERY PRODUCTION AND DISTRIBUTION IN THE SOUTHERN
CONFINES OF THE INCA EMPIRE. AN ARCHAEOLOGICAL INSIGHT TO DEFINE THE
PROVINCIAL STYLE.

M. J. Ots^{1*}, J. Buxeda i Garrigós^{2,3}, M. Madrid i Fernández^{2,3}, P. A. Cahiza⁴

1- Consejo Nacional de Investigaciones Científicas y Técnicas, Instituto Nacional de Ciencias Humanas, Sociales y Ambientales / Universidad Nacional de Cuyo, Facultad de Filosofía y Letras, Instituto de Arqueología y Etnología. Mendoza (Rca. Argentina). ORCID: 0000-0002-9002-6516

mjots@mendoza-conicet.gob.ar *Corresponding author

2- Cultura Material i Arqueometria UB (ARQUB, GRACPE), Departament d'Història i Arqueologia / Institut d'Arqueologia de la Universitat de Barcelona (IAUB), Barcelona (Catalonia, Spain).

ORCID: 0000-0001-6857-8448 jbuxeda@ub.edu.

3- Cultura Material i Arqueometria UB (ARQUB, GRACPE), Departament d'Història i Arqueologia / Institut d'Arqueologia de la Universitat de Barcelona (IAUB), Barcelona, (Catalonia, Spain).

ORCID: 0000-0003-3888-7244 mmadrid@ub.edu

4- Consejo Nacional de Investigaciones Científicas y Técnicas, Instituto Nacional de Ciencias Humanas, Sociales y Ambientales / Universidad Nacional de Cuyo, Facultad de Filosofía y Letras, Instituto de Arqueología y Etnología. Mendoza (Rca. Argentina). ORCID: 0000-0002-1574-7970

pcahiza@mendoza-conicet.gob.ar

Abstract

This paper proposes an archaeometric contribution to the study of the Inca pottery style from the southeastern frontier of *Tawantinsuyu*, also known as the Inca Empire, located in Central western Argentina (CWA). In complementing previous research, a geochemical and mineralogical characterisation of ceramics from various Inca and local sites is carried out by combining X-ray fluorescence analysis (WD-XRF), powder X-ray diffraction analysis (PXRD) and scanning electron microscopy (SEM-EDX). The exhaustive statistical treatment and discussion of the chemical data, complemented by mineralogical and microstructural data gathered through PXRD and SEM-EDX techniques, provide significant insights into the provenance of raw materials, paste recipes, firing conditions, estimated firing temperature and post-depositional contaminations. A complex structure comprising six meaningful ceramic groups has been identified, with some of them attributed to hypothetical provenance areas defined by previous research. Additionally, many ceramics remained ungrouped. Despite the identified compositional variability, certain technological attributes exhibit a

higher degree of homogeneity. The estimated firing temperature and microstructure of the pottery denote some control over firing conditions to produce vessels with high mechanical strength and toughness suitable for storage and short-distance distribution. The results of both compositional and technological analyses point to the existence of multiple production *loci* within a domestic or communitarian model of production sharing the same pottery tradition.

Keywords

Inca pottery, Central western Argentina, geochemical characterization, technology, provenance

Acknowledgments

The present paper was funded by Fondo para la Investigación Científica y Tecnológica (FONCYT, Argentina. PICT2011-0575 and PICT 2017-3169) and by the Agencia Estatal de Investigación (research project: 'Tecnolonial – Technological impact in the colonial New World. Cultural change in pottery: archaeology and archaeometry'. PID2020-117769GB-I00 MCIN/AEI/10.13039/501100011033. Spain). Consejo Nacional de Investigaciones Científicas y Técnicas (CONICET) and Secretaría de Ciencia, Técnica y Posgrado de la Universidad Nacional de Cuyo (SECTyP-UNCu) (Argentina) external fellowships were granted to the first author to collaborate with the *Cultura Material i Arqueometria UB* (ARQUB, GRACPE) research group. XRF and XRD analyses and SEM-EDX observations were conducted at the *Centres Científics i Tecnològics de la Universitat de Barcelona* (CCiTUB). J. Roberto Bárcena provided access to ceramics from Uspallata Valley. Nuria Sugrañes provided photos for Figure 2. We thank two anonymous reviewers for the insightful issues raised that have contributed to improving the paper.

AUTHOR DECLARATIONS

Statements and Declarations

All authors contributed to the study's conception and design. María José Ots and Pablo Cahiza performed material preparation, data collection and analysis. Jaume Buxeda and Marisol Madrid carried out methodology, data processing and interpretation. Jaume Buxeda, Marisol Madrid, and María José Ots wrote the first draft of the manuscript. All authors read and approved the final manuscript and commented on previous versions of the manuscript.

Competing Interests

The authors declare that they have no known competing financial interests or personal relationships that could have appeared to influence the work reported in this paper.

Ethics declarations

This manuscript has not been submitted to another journal for simultaneous consideration. It is original and has not been published elsewhere in any form or language (partially or in full).

Consent to participate/for publication

All authors agree with the content of the manuscript and give their explicit consent for its submission. Likewise, they obtained consent from the responsible authorities at the institution where the work has been carried out.

Availability of data and material

Raw data and materials are available at the INCIHUSA-CONICET laboratory (Avda. Ruiz Leal s/n, Parque Gral. San Martín. 5500. Mendoza. Rca. Argentina). WD-XRF and PXRD raw data presented in this study are openly available in the CORA.RDR, Research Data Repository (<https://dataverse.csuc.cat/>) (Buxeda et al. 2023) <https://doi.org/10.34810/data791>

Code availability

The R code for Figures 3 (variation matrix and compositional evenness graph), 5 (principal components and linear discriminant analysis) and 7A (ternary diagram) have been developed by one of us (JBG) and can be found freely available at <https://github.com/jbuxeda/ARQUB.git>.

1. Introduction

The southeastern frontier of the Inca Empire, or *Tawantinsuyu*, was located in the current territory of Central Western Argentina (CWA), which was inhabited by small-scale societies whose subsistence, technological and residential systems were impacted by the request of the expansive State between ca. 1450-1550 AD (Ots and Cahiza 2013) (Fig. 1). Inca effective occupation was materialised in the western mountain sector crossed by the Inca road system, or *Qhapac ñan*, administrative and productive centres called *tampu* and high summit sanctuaries (Bárcena 1977, among others). However, the impact of Inca imperialism exceeds these boundaries. Pottery is one of the most outstanding objects for understanding the extent and intensity of Inca interaction with local communities in this sector.

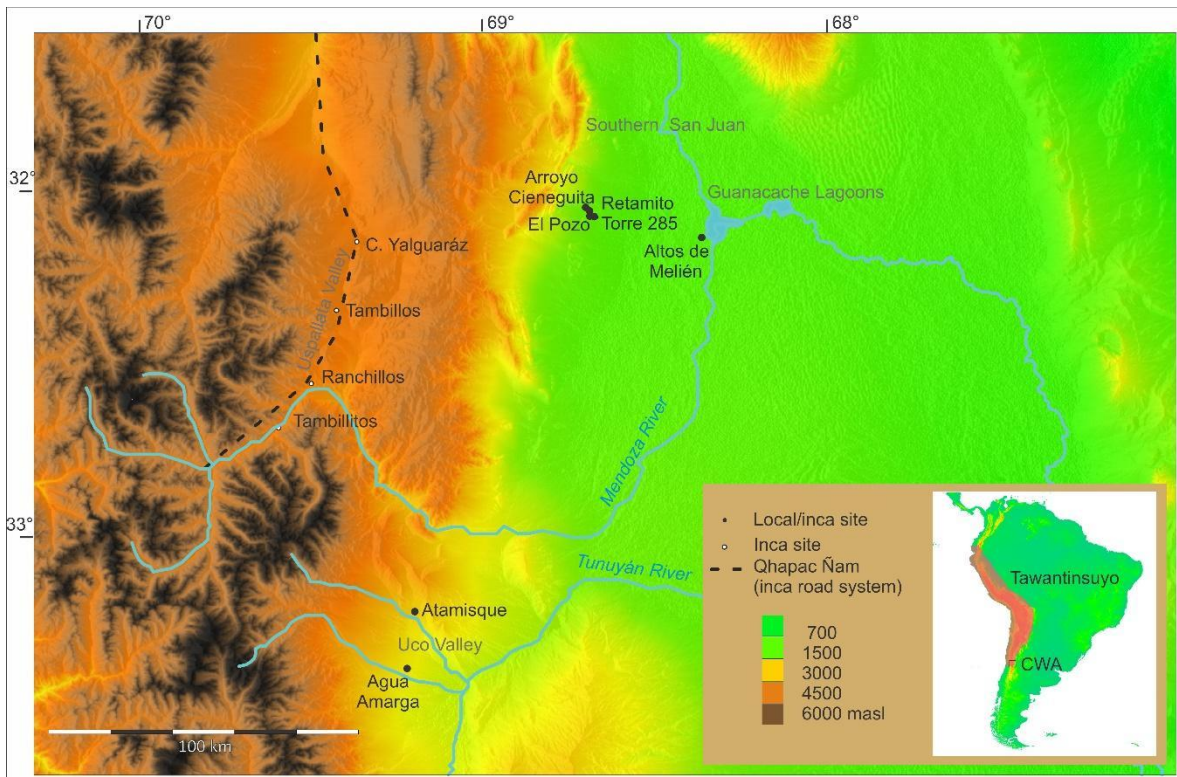


Fig. 1. Map showing the extension of the Inca Empire, or *Tawantinsuyu*. Central Western Argentina, at its southernmost east corner, is enlarged, showing all sites sampled in the present study (Geographical coordinates in Online Resource)

The first study about the ceramic component of Inca and local contemporary occupation from CWA was carried out by H. Lagiglia in the 1970s in his classification of Viluco culture, which, according

to the culture-historical paradigm, gathered a set of data from local sites, mainly funerary (Lagiglia 1978). In the following decade, a typological and archaeometric study of pottery from Inca sites highlighted the technological similarity between the Viluco style and the ceramics from a production *locus* located in the Inca *tampu* Tambillos (Bárcena y Román 1990). Currently, researchers have improved the characterisation of its morphometry (Prieto Olavarría 2012), iconographic design (Prieto Olavarría and Tobar 2017) and technological attributes through petrography of thin-sections (Carosio and Ots 2022; Prieto Olavarría and Páez 2015; Prieto Olavarría and Castro de Machuca 2017), as well as Micro Raman Spectroscopy (MRS) and Energy Dispersive X-Ray Fluorescence (EDXRF) of pigments (Tuñón López et al. 2012).

Despite the high ubiquity of this ceramic style in CWA, its frequency at archaeological sites is low. The archaeological assemblage is always highly fragmented and dispersed, except for the few documented funerary sites. This situation presents a complex challenge when attempting to address research questions about the origin of this style, how it was produced, distributed and consumed, alongside the social, economic and political practices linked to its production and use. In this paper, we propose complementing the previous research through a geochemical and mineralogical characterisation of ceramics from different Inca and local sites. By combining X-ray fluorescence, X-ray diffraction and scanning electron microscopy, we recognised technological attributes and probable areas of provenance of Provincial Inca or Viluco pottery. In this way, we contribute to creating a model for the organisation of pottery production and distribution in the southeastern frontier of the Inca Empire.

2. Archaeological background and aims

Viluco pottery has been characterised based on a repertory of 39 pieces found in local funerary sites in CWA. It exhibits a yellow-reddish colour and smooth, polished surfaces, sometimes partially covered with a slip or painted geometric patterns (Lagiglia 1978; Prieto Olavarría 2012) (Fig. 2). The ceramic set includes typical Inca fine, or ceremonial, and storage vessels. Fine pottery falls under the Inca Provincial category, imitating the Cuzco polychrome style but with less complexity or "lower quality" in terms of both shapes and decorations (according to Caldelari and Williams 1991). In Inca *tampu*, the main forms are *puco* (bowl) and *aryballos* or *urpu* (narrow-necked and flared-rim bottle) (Bárcena and Román 1990). The repertory also includes *ollas* (jars) found in local sites, a local shape considered Inca Mixto according to Caldelari and Williams' (1991) classification. In both State-affiliated and local sites, storage jars are considered utilitarian vessels (Ots and Cahiza 2013). Viluco

pottery is a minority style in residential sites, with cooking and coarse pottery being more prevalent in local sites, while other fine Inca styles, mainly Diaguita and Pacaxes, are found in Inca sites (Bárcena y Román 1990).



Fig. 2. Examples of Viluco or CWA Provincial Inca pottery. *Aryballos* or *urpu* (bottle) (**left**) and *olla* (jar) (**right**), Agua Amarga collection (Museo de Historia Natural, San Rafael). *Puco* (bowl) (**centre**), Agua Amarga (Museo Salvador Canals Frau, Facultad de Filosofía y Letras, UNCu)

Regarding the origin and changes in its production, Lagiglia (1978) proposed an Andean yet pre-Inca origin based on diffusionist theory, which was later transformed by Inca and Spanish colonisation. However, subsequent studies, supported by an increase in investigated sites and absolute dates in the following decades, favour the Inca origin of this style (García 1996; Ots 2008; Prieto Olavarría 2012). The iconographic attributes of the design also align with Inca influence (García 1996; Prieto Olavarría and Tobar 2017). Additionally, a technological breakthrough was identified regarding the local precedent ceramics (Carosio and Ots 2020, 2022). For this reason, we believe that Viluco is the Inca style in CWA, and we will refer to this style as CWA Provincial Inca (CWA-PI).

Despite its prevalence, little is known about the production areas of CWA-PI ceramics due to the low resolution of material evidence. The pottery was fired in ephemeral structures of open firing in a primitive cooking mode A of reducing firing and oxidising post-firing (Picon 1973). These firing practices do not leave structures preserved in the archaeological record. Nevertheless, archaeological

evidence suggests two regional production centres: one in Tambillos *tampu* and one at the local site RT285. Bárcena and Román (1990) proposed that ceramic production occurred in one sector of the Tambillos *tampu*, in Uspallata Valley (Fig. 1), where a community of potters (*mitmaqkuna*) would have been led by specialised craftsmen known as *sañucamayoc*. This organisational model aligns with the proposed model for pottery production and distribution in *Tawantinsuyu* (Alconini 2013; Davenport 2020; D'Altroy et al. 1994; Hayashida 1999; Murra 2002 [1978], among others). Although no firing structure was recorded on the site, tools (slate straighteners), wasters and raw materials such as quartz, calcite and pigments were recovered inside one of the habitation structures.

Moreover, preliminary archaeometric characterisation of raw materials and pottery –using petrography by optical microscopy on thin sections, x-ray diffraction analysis and atomic absorption spectrophotometry– also supported this identification as a ceramic production site (Bárcena and Román 1990). Another production *locus* was proposed at the local site of RT285, in the eastern foothills south of San Juan province (Fig. 1) (Ots and Cahiza 2016). Firing structures were recovered at this site, and the shape, size and estimated firing temperature of its walls seem to be related to pottery production. Additionally, vitrified pottery remains were also recovered with high frequency. This evidence and the availability of necessary natural resources –clay, water, fuel and weather conditions– further support the expected needs and traces of such pottery production.

The existence of pottery production at these sites and other potential areas has been explored through petrographic characterisation by thin-section. Thus, a study conducted through a petrographic examination of ceramics from Inca and early colonial contexts in the Huentota Valley and samples from isolated outcrops identified at least two sources of temper located near the sites. This suggests the possibility of another production area in the Huentota Valley (Prieto Olavarría and Castro de Machuca 2017). Likewise, the technological and compositional features of pottery recovered at Agua Amarga, in Uco Valley, were explored and compared with those recovered at Uspallata Valley and southern San Juan sites (Carosio and Ots 2022; Ots 2008). In that case, the results reveal significant compositional diversity and heterogeneity but present more uniformity in pastes in both Uspallata Valley and southern San Juan sets, showing a clear correlation with local geology and suggesting decentralised local production in both areas (Carosio and Ots 2022).

As detected in funerary contexts, fine CWA-PI pottery was a valuable good that also worked as an identity marker. Similar to other ancient estates, the production and circulation of such goods were mechanisms of control and power (Shortman and Urban 2004), linked to Andean political and economic relations of reciprocity. While little is known about the socio-political organisation of the local communities and their interactions with the expansive State in CWA, ceramic production and

use were strongly tied to the political economy. Therefore, studying this pottery style can provide proxies for knowing other dimensions of society (D'Altroy and Earle 1990; Rice 2010; Shortman and Urban 2004).

Previous research has improved our knowledge about the macroscopic and microscopic attributes of this technological style. However, exploring the chemical and mineralogical composition features could contribute to shedding light on decisions regarding raw material procurement, paste processing and firing technology. To this end, the present paper explores the archaeometric characterisation of CWA-PI pottery from different sectors of CWA, particularly the Uco and Uspallata valleys and the eastern foothills south of San Juan Province (Fig. 1). The results reveal that, contrary to the expectations for the centralised pottery production and distribution model proposed for other imperial provinces (Alconini 2013; D'Altroy et al. 1994; De la Fuente et al. 2015, among others), in this peripheral and remote area, multiple production centres were working simultaneously. This finding explains the variability of paste treatments for similar vessels, corresponding to a small scale and community level of production.

3. Materials and methods

3.1. Materials

For the analytical program of this study, archaeological ceramics unearthed at twelve Inca and local indigenous sites of CWA were sampled (Table 1, Fig. 1). These sites can be grouped into three different areas. The first one is Uspallata Valley, where all but one are Inca sites. The Inca sites included in the present study, from north to south, are called Ciénaga de Yalguaraz, *tampu* Tambillos, Ranchillos and Tambillitos. Potrero Chanchería is located in the same valley but lacks Inca architecture. The other two areas are the foothills and plains south of San Juan province (sites RT285, Retamito, El Pozo, Altos de Melián and Arroyo Cieneguita) and Uco Valley (Agua Amarga and Atamisque sites), located respectively to the east and south of the *Qhapac ñan* system. The sites in these areas lack Inca infrastructure but are integrated into their economic networks.

The studied sample consists of 85 ceramic individuals, along with 2 experimental ceramics prepared from clays collected at Ranchillos (MDZ140) and RT285 (MDZ149), and 1 firing structure unearthed at RT285 (MDZ150). The experimental ceramics and firing structure were included to gather information about the available clays in the area. Out of the 85 ceramic individuals, 22 were unearthed from sites in Uco Valley, 35 in Uspallata Valley (plus the MDZ140 experimental ceramics), and 28

from sites in the foothills south of San Juan province (plus the MDZ149 experimental ceramics and the MDZ150 firing structure). The sample includes the possible production centres of Tambillos and RT285, their potential distribution channels, and examples of both types of Inca provincial pottery (fine or ceremonial vessels –*urpu*, *ollas* and *pucos*, Fig. 2–, and utilitarian storage vessels). The paste of CWA Provincial pottery exhibits a high degree of heterogeneity regarding the size and distribution of aplastic inclusions and colour (Carosio and Ots 2022). However, the pottery recovered from the *tampu* is more standardised than the one recovered from local sites, with some ceramics resembling those from the *tampu*, but others displaying differences in several attributes.

Site	Area	Types	Sample number	Comments
Agua Amarga (Ots, 2008) (n = 20)	Uco Valley (west-central Mendoza)	<i>Aryballos or urpu</i>	MDZ026 (CGI01), 30 (CGI01), 46 ^{PE} (CGI01, PF1)	red slip (MDZ030, 46)
		<i>Puco</i>	MDZ025 (CGI02), 29 (CGI01), 45 (CGI03)	red slip (MDZ025, 29), black painted (MDZ045)
		<i>Olla</i>	MDZ027 (CGI02), 28 (Ung), 31 (Ung), 38 (CGI05), 39 (Ung), 151 (CGI05)	red painted (MDZ028), red/black painted (MDZ038), orange slip (MDZ151)
		Storage jar	MDZ032 (Ung), 37 (CGI01), 40 (Ung), 41 (CGI02), 42 (CGI03), 43 (CGI05), 112 ^{PE} (CGI01, PF5), 113 (CGI01)	red slip (MDZ037)
Atamisque (Canals Frau 1950) (n = 2)	Uco Valley (west-central Mendoza)	<i>Aryballos or urpu</i>	MDZ110 (Ung), 111 (CGI01)	
Potrero Chanchería (Bárcena 1977; Terraza, Bárcena 2016) (n = 14)	Precordilleran Uspallata Valley (northwest Mendoza)	<i>Aryballos or urpu</i>	MDZ050 ^{PE} (CGI03, PF1), 53 (CGI02), 54 (CGI02), 59 (CGI02)	red slip (MDZ050, 59), brown painted (MDZ054)
		<i>Puco</i>	MDZ055 (CGI03), 56 (CGI06)	red slip (MDZ055, 56)
		<i>Olla</i>	MDZ052 ^{PE} (CGI06, PF8), 57 ^{PE} (CGI03, PF4)	red slip (MDZ052)
		Storage jar	MDZ047 (CGI02), 48 (Ung), 49 (CGI02), 51 (CGI02), 58 (CGI02), 108 (CGI03)	
Tambillos (I. s.) (p. c.) (Bárcena, Román 1990) (n = 12)	Precordilleran Uspallata Valley (northwest Mendoza)	<i>Puco</i>	MDZ072 (CGI02)	
		<i>Olla</i>	MDZ069 ^{PE} (CGI06, PF8), 75 (CGI02)	red slip (MDZ075)
		Storage jar	MDZ060 ^{PE} (CGI03, PF1), 61 ^{PE} (CGI02, PF1), 62 (CGI02), 63 (CGI02), 64 (CGI02), 65 (CGI02), 66 ^{PE} (CGI02, PF4), 67 (Ung), 68 ^{PE} (CGI02, PF4)	red slip (MDZ067)
Ciénaga Yalguaraz (I. s.) (Bárcena 1977) (n = 4)	Precordilleran Uspallata Valley (northwest Mendoza)	<i>Olla</i>	MDZ070 (Ung), 71 (Ung)	
		Storage jar	MDZ073 ^{PE} (CGI02, PF4), 74 (CGI02)	

Ranchillos (I. s.) (Bárcena 1998) (n = 1)	Precordilleran Uspallata Valley (northwest Mendoza)	Experimental sample	MDZ140 (Ung)	modelled and fired clay
Tambillitos (I. s.) (Bárcena 1977) (n = 5)	Precordilleran Uspallata Valley (northwest Mendoza)	<i>Aryballos or urpu</i>	MDZ076 ^{PE} (CGI02, PF4), 77 (CGI02), 79 ^{PE} (CGI02, PF4), 109 (CGI02)	brown slip (MDZ109)
		<i>Olla</i>	MDZ080 (CGI02)	
Altos de Melién (Cahiza 2003) (n = 4)	Lagunas de Guanacache (north Mendoza)	<i>Olla</i>	MDZ087 ^{PE} (CGI05, PF6), 88 (Ung), 89 (CGI05)	
		Storage jar	MDZ090 (CGI03)	
RT285 (p. c.) (Cahiza 2003) (n = 11)	Foothills (south San Juan)	<i>Olla</i>	MDZ092 ^{PE} (CGI03, PF6), 93 ^{PE} (CGI05, PF6), 95 (CGI03), 98 (CGI05), 99 (CGI05), 102 (CGI05), 104 (CGI02)	
		Storage jar	MDZ094 (CGI05), 101 (CGI02)	
		Firing structure	MDZ150 (Ung)	
		Experimental sample	MDZ149 (CGI05)	modelled and fired clay
El Pozo (Cahiza 2003) (n = 4)	Foothills (south San Juan)	<i>Olla</i>	MDZ086 (Ung), 97 (CGI02)	
		Storage jar	MDZ085 ^{PE} (CGI05, PF6), 103 (CGI02)	
Arroyo Cieneguita (Cahiza 2003) (n = 2)	Foothills (south San Juan)	<i>Olla</i>	MDZ100 ^{PE} (CGI05, PF6), 105 ^{PE} (CGI03, PF6)	incised (MDZ100)
Retamito (Cahiza 2003) (n = 9)	Foothills (south San Juan)	<i>Aryballos or urpu</i>	MDZ081 ^{PE} (CGI05, PF6), 83 (CGI02), 84 (Ung), 91 ^{PE} (CGI03, PF6), 136 ^{PE} (CGI04, PF2)	red painted (MDZ081, 83), white painted (MDZ091)
		<i>Puco</i>	MDZ135 (CGI04)	black painted (MDZ135)
		<i>Olla</i>	MDZ082 ^{PE} (CGI05, PF6), 106 ^{PE} (CGI04, PF2), 107 (CGI05)	red/black painted (MDZ106), incised (MDZ107)

Table 1 Sites and individuals sampled in the present study. References to relevant archaeological studies are indicated. (I. s.): Inka site; (p. c.): production centre; (Ung): ungrouped; ^{PE}: individuals previously characterised by thin-section petrography (Carosio and Ots 2022). In parenthesis after individual label, group after chemical characterisation (CG) and petrofabric (PF)

3.2. Analytical methods

The chemical characterisation of the 88 individuals was performed using wavelength-dispersive X-ray fluorescence (WD-XRF) analysis. Samples of about 15 g were taken from each individual. The superficial layers were mechanically removed, and the samples were milled in a tungsten carbide cell mill Spex Mixer mod. 8000. The chemical composition was determined from powder previously dried

in an oven for 12 h at 105 °C. Two 30 mm glass bead replicates were made by mixing 0.3 g of dried sample with 5.7 g of lithium tetraborate ($\text{Li}_2\text{B}_4\text{O}_7$) flux (1/20 dilution) and 5 mg of lithium iodide (LiI) as a release agent to determine the major and minor elements. This mixture was homogenised, deposited in a 95%Pt-5%Au crucible and melted in a fully automatic bead preparation system, PANalytical Perl'X-3 at 1125 °C. Pressed powder pellets were made using 6 g of specimen mixed with 2 ml of a binding agent solution of n-butyl methacrylate synthetic resin (Elvacite® 2044) in acetone at 20% by mass to determine trace elements. This mixture was manually homogenised in an agate mortar to dryness and placed on a base of boric acid (H_3BO_3) in an aluminium vessel of 40 mm diameter that was subjected to a pressure of 200 kN for a period of 60 s using a Herzog press. The concentrations were quantified using an Axios^{mAX}-Advanced PANalytical spectrometer with an Rh excitation source calibrated by 56 international Geological Standards. Interferences were considered, and matrix effects were corrected using the PANalytical Pro-Trace software for trace elements. The elements determined were: Na₂O, MgO, Al₂O₃, SiO₂, P₂O₅, K₂O, CaO, TiO₂, V, Cr, MnO, Fe₂O₃ (as total Fe), Co, Ni, Cu, Zn, Ga, Rb, Sr, Y, Zr, Nb, Mo, Sn, Ba, Ce, W, Pb and Th. Major and minor elements are expressed as concentrations of oxides in mass fraction percentage (w%). Trace elements are expressed as concentrations of elements in mass fraction (mg/kg). Loss on ignition (LOI) (expressed as w%) was determined by firing 0.3 g of the dried specimen at 950 °C for 3 h. Calcinations were carried out in a Heraeus muffle model M-110, using a heating rate of 3.4 °C/min and free cooling. The concentrations of Mo and Sn were discarded due to analytical imprecision. Co and W were also discarded due to possible contamination from the tungsten carbide cell mill. Similarly, P₂O₅, Cu and Pb concentrations were not used in the data treatment because few values were considered erratic. Such values can be attributed to contaminations during burial, such as P₂O₅ from organic matter (Buxeda 1999). However, the general influence of these three elements was low, and the main structure defined in the data set was preserved after discarding them. Finally, LOI was not used in the data treatment. The need to calculate the LOI and how the logratio analysis overcomes the scale effect, a dilution effect, has already been discussed elsewhere (Buxeda 1999).

Mineralogical characterisation of the 88 individuals was performed using powder X-ray diffraction (PXRD). The previously prepared powder specimens were manually side-loaded and pressed with frosted glass into a cylindrical sample holder. Measurements were conducted using a Bragg-Brentano geometry diffractometer, PANalytical X'Pert PRO MPD Alpha-1 (radius = 240 mm), employing Ni-filtered Cu K α radiation ($\lambda = 1.5418 \text{ \AA}$) at a working power of 45 kV and 40 mA. The diffractometer was equipped with an X'Celerator detector (active length = 2.122°). Measurements were taken in the range of (5 to 80)°2 θ with a 0.026° step size and an acquisition time of 50 s, spinning the sample at 1 Hz. The crystalline phases in each analysed specimen were evaluated using the PANalytical X Pert

HighScore Plus software package, which includes the Powder Diffraction File™ (PDF®) from the International Centre for Diffraction Data (ICDD).

Finally, in a multi-phase sampling approach, a subsample, guided by the stratification revealed by XRF and XRD analysis in terms of meaningful compositional groups and mineralogical fabrics, as well as specimen availability (Buxeda and Madrid 2017), underwent further examination using SEM-EDX. This subsample comprises 17 individuals, as specified in the technical section below. SEM observations were performed on fresh cross-section fractures passing through the oro-aboral axis of the body wall to observe the microstructure, estimate the degree of sintering and vitrification stage of the matrix, and facilitate microanalysis of interesting features. These observations were carried out using a JEOL JSM-6510 scanning electron microscope (SEM) coupled with an energy dispersion X-ray spectroscopy analyser (EDX) INCA Energy 250 (Oxford Instruments). Bulk specimens were fixed on metal specimen stubs using silicone adhesive, and non-conductive ceramic specimens were rendered conductive. Colloidal silver paint was applied to the excess silicone adhesive and lateral sides of the ceramic bulk specimens. Subsequently, the specimen surface was coated with a thin carbon film (~ 10 nm) via vacuum evaporation. The observations were conducted with an acceleration voltage of 20 kV and a working distance of 10 mm.

It is important to emphasise that 24 samples had previously undergone thin-section petrographic analysis (Carosio and Ots 2022). The results from these analyses will be discussed in conjunction with the geochemical and mineralogical characterisation presented in this paper.

3.3. Statistical methods

The elemental concentrations of the individuals analysed by XRF (Table 2) correspond to a particular case of the projective $d+1$ -dimensional space, where the projective points are projected onto the simplex \mathbb{S}^d and are represented by homogeneous coordinates that have a constant sum k ($k \in \mathbb{R}_+$),

$$C(\mathbf{w}) = \mathbf{x} = [x_1, \dots, x_d, x_{d+1}] \mid x_i \geq 0 \ (i = 1, \dots, d, d+1), x_1 + \dots + x_d + x_{d+1} = k$$

(in this case, $k = 100$). The vector space of the projective points is the positive orthant. Hence, for statistical data treatment, raw concentrations have been alr (additive log-ratio) transformed according to:

$$\mathbf{x} \in \mathbb{S}^d \rightarrow \mathbf{y} = \ln\left(\frac{x_d}{x_{d+1}}\right) \in \mathbb{R}^d \quad (\text{Equation 1}),$$

being S^d the d -dimensional simplex and $\mathbf{x}_d = [x_1, \dots, x_d]$. They have also been clr (centred log-ratio) transformed following the equation:

$$\mathbf{x} \in S^d \rightarrow \mathbf{z} = \ln\left(\frac{\mathbf{x}}{g(\mathbf{x})}\right) \in H \subset \mathbb{R}^{d+1} \quad (\text{Equation 2}),$$

being S^d the d -dimensional simplex, $g(\mathbf{x})$ the geometric mean of all $d+1$ components of \mathbf{x} , and $H \subset \mathbb{R}^{d+1}$ a hyperplane vector subspace of \mathbb{R}^{d+1} (Aitchison 1986; Buxeda 1999, 2018; Egozcue and Pawlowsky-Glahn 2011; Martín-Fernández et al. 2015; van de Boogaart and Tolosana-Delgado 2013).

The statistical treatment of the chemical data was performed on the retained values using R (R Core Team, 2021).

4. Results and discussion

4.1. Chemical characterisation

The initial analysis calculated the variation matrix, whose columns represent all possible variances of alr-transformed data (Equation 1), using each retained component as the divisor. This matrix comprehensively defines the covariance structure of the compositional data and provides the total variation (tv) of the analysed ceramic assemblage (Aitchison 1986). In this case, the total variation is 1.02 (Fig. 3), possibly suggesting the existence of a polygenic group (Buxeda and Kilikoglou 2003).

Ic	Na ₂ O	MgO	Al ₂ O ₃	SiO ₂	P ₂ O ₅	K ₂ O	CaO	TiO ₂	V	Cr	MnO	Fe ₂ O ₃	Co	Ni	Cu	Zn	Ga	Rb	Sr	Y	Zr	Nb	Mo	Sn	Ba	Ce	W	Pb	Th	LOI
MDZ025	2.00	3.08	15.75	61.60	0.23	3.84	4.21	0.64	88	24	0.13	5.51	35	20	54	116	23	148	370	35	230	13	2	5	542	77	206	25	16	1.72
MDZ026	1.92	2.52	18.20	61.83	0.24	3.66	1.31	0.80	149	60	0.12	6.65	21	41	92	198	26	152	221	35	184	14	2	6	793	70	126	45	15	2.70
MDZ027	2.60	2.63	15.59	62.34	0.27	3.19	4.70	0.67	98	31	0.13	5.83	22	22	41	104	21	123	373	32	199	11	1	4	618	70	233	22	12	0.99
MDZ028	2.49	1.94	15.80	66.03	0.15	3.76	2.70	0.56	77	37	0.10	4.73	28	22	28	109	24	209	164	57	218	22	1	7	440	96	532	25	29	0.83
MDZ029	1.86	3.04	18.00	62.79	0.25	3.39	1.34	0.81	123	54	0.14	6.58	24	34	46	156	24	145	247	32	196	13	2	4	675	71	207	38	14	1.55
MDZ030	1.57	2.58	18.68	60.38	0.24	4.05	1.02	0.82	152	64	0.12	7.08	20	49	102	244	26	154	170	33	175	14	2	6	807	69	50	49	14	2.55
MDZ031	2.46	1.36	18.62	60.23	0.11	2.60	3.13	0.80	121	24	0.15	7.19	24	14	92	158	21	77	238	39	216	7	1	2	609	46	256	47	12	3.06
MDZ032	2.97	2.29	15.66	66.45	0.23	2.71	1.62	0.72	94	58	0.11	4.97	14	24	62	112	20	97	331	24	190	10	2	3	726	50	64	26	11	1.51
MDZ037	1.81	2.59	18.96	59.11	0.18	3.99	2.83	0.82	145	74	0.16	7.18	25	54	77	188	26	166	205	31	165	14	1	5	866	72	203	41	14	1.72
MDZ038	2.56	2.84	15.89	62.86	0.21	3.20	3.50	0.72	103	55	0.12	6.05	22	25	33	100	21	127	356	31	209	12	1	3	648	72	230	22	14	1.14
MDZ039	2.50	1.89	15.27	65.45	0.15	3.06	1.87	0.67	66	30	0.09	4.72	11	17	37	81	17	85	260	22	180	8	1	3	534	49	94	20	8	2.83
MDZ040	2.27	2.76	16.50	63.11	0.26	3.51	3.96	0.50	66	40	0.12	4.60	14	14	40	125	21	111	259	25	158	10	2	3	588	66	80	28	13	1.76
MDZ041	2.21	2.96	16.20	62.14	0.30	3.60	4.69	0.68	93	40	0.13	5.96	17	22	45	119	22	135	382	32	203	12	1	5	598	78	80	26	14	1.78
MDZ042	2.77	3.16	16.24	61.91	0.19	3.36	2.98	0.74	103	30	0.14	6.28	16	21	41	100	22	125	320	31	204	12	2	4	528	72	42	22	13	1.80
MDZ043	2.38	2.55	16.60	63.22	0.23	3.76	2.82	0.78	100	45	0.11	6.30	20	26	40	114	22	137	206	35	199	13	1	5	627	78	136	28	14	0.95
MDZ045	2.84	2.85	16.02	63.25	0.21	3.55	3.25	0.66	88	30	0.12	5.64	18	18	31	95	22	139	238	34	197	12	2	3	461	69	175	24	14	1.04
MDZ046	2.09	2.38	19.27	59.27	0.24	3.88	2.23	0.82	156	72	0.15	7.34	21	49	84	186	26	146	265	31	164	12	1	4	925	66	70	40	14	1.55
MDZ047	2.43	3.52	16.45	60.98	0.25	3.49	4.22	0.68	95	22	0.12	5.88	16	19	42	102	22	133	358	32	201	12	2	4	540	76	61	23	14	1.36
MDZ048	2.42	3.10	16.42	59.19	1.19	3.45	3.37	0.67	94	29	0.14	5.82	15	18	45	95	22	122	452	30	200	12	2	4	912	70	35	25	13	3.62
MDZ049	2.63	3.30	16.82	59.84	0.42	3.43	4.33	0.68	95	27	0.12	6.05	17	19	37	104	24	146	367	31	194	12	1	2	676	71	69	20	14	1.68
MDZ050	2.36	2.99	17.35	61.36	0.24	3.78	2.64	0.69	100	29	0.13	6.32	18	22	50	122	25	158	260	32	199	13	2	4	554	84	59	32	14	1.63
MDZ051	2.00	3.23	16.23	60.50	0.24	3.16	5.75	0.66	96	34	0.12	5.71	16	19	47	100	22	137	471	32	195	12	1	4	763	72	60	22	14	1.48
MDZ052	2.23	1.52	15.73	65.54	0.15	3.37	1.70	0.66	83	21	0.06	4.82	11	11	99	104	21	117	239	32	227	12	1	5	905	80	71	35	14	2.69
MDZ053	2.17	3.21	16.12	60.30	0.25	3.37	4.78	0.67	94	20	0.14	5.87	16	17	64	98	21	115	455	30	190	11	1	3	630	62	73	22	12	2.18
MDZ054	2.59	3.26	16.37	60.64	0.32	3.59	4.80	0.66	79	21	0.13	5.70	17	16	29	88	22	133	338	32	190	12	1	3	689	76	77	17	13	1.10
MDZ055	2.23	3.24	16.24	60.10	0.18	3.71	2.71	0.66	89	17	0.12	5.77	14	16	63	89	21	112	257	28	176	10	1	4	574	60	40	23	12	3.42
MDZ056	1.97	1.77	18.20	64.56	0.16	4.00	1.62	0.61	97	16	0.05	5.01	14	11	33	154	25	152	200	37	212	13	2	6	730	83	113	44	16	1.20
MDZ057	2.66	2.38	16.09	64.31	0.14	3.63	2.68	0.62	84	29	0.11	5.23	14	16	32	100	22	144	267	30	197	12	1	4	562	72	139	28	14	1.20
MDZ058	2.30	3.12	16.04	60.66	0.51	3.29	5.42	0.67	89	25	0.12	5.79	16	17	33	94	21	123	470	29	194	11	1	3	634	72	123	20	12	1.42
MDZ059	2.24	3.37	16.46	60.74	0.23	3.12	5.88	0.67	95	26	0.12	5.97	35	19	31	95	22	125	449	31	197	12	2	4	515	68	460	21	14	0.84
MDZ060	2.48	3.25	16.80	60.70	0.19	3.40	2.83	0.66	95	22	0.11	5.96	15	18	33	106	23	134	277	27	180	11	1	4	527	71	64	26	13	3.24
MDZ061	2.38	3.38	16.51	58.98	0.62	3.74	5.12	0.68	84	28	0.14	6.11	17	19	29	95	21	126	398	31	189	11	1	4	496	74	69	16	14	2.18
MDZ062	2.37	3.16	16.11	61.05	0.38	3.63	4.21	0.68	98	22	0.11	5.84	15	18	32	96	21	117	335	30	195	11	1	4	556	68	53	21	12	2.05
MDZ063	2.25	3.16	15.66	59.73	0.50	3.17	5.42	0.64	92	21	0.12	5.64	14	17	31	85	22	118	444	30	192	11	1	5	556	56	60	15	13	2.72
MDZ064	2.28	3.21	16.23	61.06	0.63	3.45	5.05	0.66	90	20	0.12	5.95	17	17	31	80	22	120	389	30	197	12	1	3	519	67	102	17	14	1.19
MDZ065	2.40	3.16	16.20	61.25	0.30	3.15	4.99	0.65	94	21	0.13	5.65	15	17	28	94	22	124	407	31	194	12	2	2	621	70	65	20	13	1.56
MDZ066	2.09	3.19	15.86	59.78	0.34	3.45	4.86	0.64	93	17	0.12	5.51	13	16	29	95	22	115	402	30	192	11	2	4	570	64	29	21	13	3.49
MDZ067	2.36	2.55	15.88	66.82	0.18	4.12	1.43	0.58	63	53	0.08	4.70	28	17	16	88	20	160	176	33	192	12	1	4	416	84	230	22	14	0.67
MDZ068	2.22	3.10	16.13	61.03	0.25	3.15	4.45	0.66	96	20	0.13	5.62	16	17	28	96	22	121	402	32	195	12	2	4	566	69	52	22	16	2.72
MDZ069	2.46	1.87	16.23	65.36	0.19	3.54	1.99	0.64	88	26	0.08	5.87	20	14	22	107	21	134	274	35	208	12	1	3	678	74	244	33	14	1.35
MDZ070	2.73	2.12	17.84	59.59	0.24	3.13	5.86	0.61	96	29	0.15	5.25	15	16	30	122	24	140	666	24	150	10	3	4	744	62	100	31	12	1.56
MDZ071	2.66	2.15	17.99	59.92	0.26	3.25	5.53	0.62	96	28	0.15	5.30	18	16	29	124	24	143	661	25	158	10	3	3	771	69	164	30	14	1.47
MDZ072	2.54	3.71	16.66	61.02	0.23	3.48	4.11	0.70	88	24	0.12	6.01	18	19	33	98	23	136	372	32	202	12	1	2	495	77	107	20	14	0.87
MDZ073	2.54	3.21	15.96	59.53	0.26	3.12	5.42	0.64	90	26	0.12	5.61	19	17	36	90	22	127	458	32	195	12	1	2	501	76	76	19	14	3.16
MDZ074	2.42	3.27	15.96	59.48	0.33	3.17	6.31	0.64	92	27	0.12	5.62	16	17	29	89	22	126	478	31	198	12	1	2	470	67	58	18	14	2.04

MDZ075	2.02	3.33	16.27	60.12	0.40	3.13	5.87	0.66	97	26	0.12	5.90	17	18	34	97	22	125	497	31	198	11	1	4	615	70	96	19	13	1.43
MDZ076	2.37	3.50	16.18	60.16	0.26	3.52	5.10	0.66	86	21	0.13	5.80	16	18	30	88	22	133	430	32	196	12	1	4	525	73	94	18	14	1.66
MDZ077	2.12	3.30	16.21	61.20	0.26	3.24	5.18	0.66	87	20	0.12	5.71	17	17	33	90	22	126	450	31	203	12	1	3	546	70	101	19	14	1.24
MDZ079	2.05	3.36	16.40	61.19	0.23	3.25	5.38	0.67	93	22	0.12	5.77	17	18	31	87	23	130	481	32	207	12	1	5	568	75	78	16	14	0.89
MDZ080	1.94	3.60	16.31	59.02	0.24	3.12	6.37	0.66	100	19	0.12	6.12	17	18	35	99	23	122	515	31	192	11	1	2	556	74	62	19	14	2.15
MDZ081	1.62	3.42	18.79	57.98	0.23	4.04	3.74	0.80	111	39	0.14	7.70	20	28	42	146	28	160	247	37	201	14	1	4	611	95	70	37	16	1.06
MDZ082	2.49	2.56	15.87	62.89	0.20	3.29	3.05	0.73	113	44	0.11	6.21	18	24	26	102	22	114	276	31	183	12	2	4	669	65	119	22	12	1.51
MDZ083	2.42	3.37	16.54	61.08	0.24	3.48	4.34	0.66	91	24	0.11	5.88	18	19	29	93	23	143	387	33	205	13	1	5	522	75	85	19	14	1.13
MDZ084	2.99	2.98	18.01	61.75	0.11	3.93	0.86	0.55	56	18	0.07	5.38	12	16	17	95	24	143	97	51	204	16	1	4	301	100	76	28	19	2.27
MDZ085	2.58	3.43	16.69	57.90	0.22	3.65	4.35	0.70	116	45	0.13	6.62	16	25	46	129	26	134	145	32	182	12	1	3	456	78	49	25	14	3.04
MDZ086	3.02	2.61	15.54	62.12	0.27	4.18	3.81	0.76	71	20	0.11	5.38	13	12	21	92	22	144	346	36	300	13	1	5	874	86	95	20	16	1.20
MDZ087	2.02	3.36	16.21	55.19	0.19	3.56	5.87	0.62	107	36	0.12	6.03	15	23	40	116	25	141	349	28	161	10	1	5	458	64	28	24	13	5.96
MDZ088	2.12	2.64	17.54	62.06	0.13	3.73	2.38	0.82	130	44	0.07	5.95	16	20	30	108	24	146	322	29	199	13	4	3	649	64	131	28	14	1.83
MDZ089	1.77	3.12	16.74	53.57	0.19	3.41	6.78	0.71	126	50	0.13	6.67	19	33	37	111	23	139	344	32	167	12	2	4	731	72	31	24	14	5.62
MDZ090	2.54	3.16	15.90	60.85	0.24	3.26	3.67	0.70	100	25	0.13	6.19	16	20	28	106	22	118	235	31	184	12	2	4	545	63	90	23	13	2.36
MDZ091	2.60	2.76	15.72	63.64	0.20	2.98	3.64	0.66	91	20	0.13	5.46	16	16	30	104	21	111	219	30	183	11	1	4	536	72	106	28	12	1.13
MDZ092	2.54	2.94	16.16	62.81	0.27	3.18	3.13	0.70	93	26	0.12	6.04	17	21	29	106	21	116	254	28	175	12	1	2	516	62	68	28	12	1.42
MDZ093	1.79	3.17	18.06	59.84	0.22	3.59	3.26	0.81	143	60	0.13	7.59	21	33	38	122	26	149	202	35	185	14	1	5	659	78	145	26	15	0.74
MDZ094	1.61	3.33	18.70	58.04	0.22	3.80	3.57	0.78	123	41	0.13	7.56	20	28	38	142	28	163	237	36	198	14	1	4	569	83	50	37	15	1.12
MDZ095	1.92	3.62	16.85	57.21	0.21	2.96	4.30	0.72	118	22	0.14	7.28	18	25	38	122	25	128	247	32	188	12	2	4	488	79	18	29	14	3.60
MDZ097	2.34	2.96	15.43	59.81	0.20	3.04	5.12	0.70	94	21	0.11	5.80	14	18	29	92	20	96	352	26	171	10	1	2	588	59	27	20	10	3.25
MDZ098	1.82	3.16	18.00	59.88	0.23	3.58	3.34	0.82	135	54	0.13	7.57	20	31	40	118	24	144	200	34	180	13	1	3	623	83	111	24	14	0.81
MDZ099	1.94	3.16	17.99	59.84	0.23	3.68	3.36	0.81	137	60	0.13	7.52	21	32	37	121	25	146	207	35	186	14	1	4	621	78	122	24	16	0.70
MDZ100	1.59	3.02	16.22	59.03	0.19	3.21	5.11	0.74	124	44	0.12	6.90	18	28	34	104	23	126	186	31	171	12	1	5	597	74	75	22	13	2.91
MDZ101	2.34	2.87	15.93	63.38	0.25	3.54	4.04	0.64	81	25	0.11	5.19	14	15	27	89	21	149	412	32	210	13	1	3	545	74	92	23	14	0.90
MDZ102	2.26	2.98	17.15	60.31	0.41	3.52	3.69	0.72	108	37	0.20	6.60	18	23	34	118	23	130	160	32	181	12	1	5	568	78	79	28	14	1.41
MDZ103	2.13	3.38	16.29	59.22	0.38	3.61	4.33	0.68	95	23	0.12	5.93	14	19	42	102	22	121	360	30	193	12	1	5	562	70	46	24	14	2.69
MDZ104	2.53	2.62	15.13	62.22	0.27	3.18	4.80	0.66	82	28	0.12	5.52	15	17	33	87	20	106	314	27	180	11	1	2	588	62	101	20	11	1.61
MDZ105	2.05	2.95	15.02	59.27	0.23	2.96	4.27	0.67	102	21	0.10	6.39	16	21	24	104	21	104	230	30	173	10	1	5	553	66	35	21	12	4.56
MDZ106	2.88	2.51	15.62	63.87	0.19	3.59	3.46	0.56	71	26	0.14	5.17	14	15	28	109	22	159	288	39	272	17	1	3	461	86	119	26	25	0.86
MDZ107	1.92	3.08	17.57	58.66	0.22	3.48	4.13	0.75	119	42	0.12	6.97	18	26	37	113	25	134	206	31	168	12	1	5	542	72	94	25	14	1.60
MDZ108	2.49	3.14	16.55	61.21	0.26	3.77	3.17	0.65	90	30	0.12	5.76	16	19	39	108	23	143	300	32	204	12	1	4	588	74	97	22	14	1.52
MDZ109	2.36	3.33	16.09	60.04	0.22	3.29	5.80	0.68	94	27	0.12	5.83	17	18	27	94	21	116	457	30	196	11	1	2	488	68	121	20	13	1.10
MDZ110	1.62	2.85	20.23	59.03	0.17	4.27	0.64	0.86	166	68	0.19	7.72	22	49	55	240	28	177	115	36	167	14	2	4	954	77	82	50	16	1.48
MDZ111	2.00	2.34	18.65	61.22	0.20	3.80	1.48	0.80	145	60	0.14	6.68	20	43	62	182	26	151	250	31	175	14	3	3	1019	66	107	41	14	1.23
MDZ112	1.40	2.42	16.86	59.84	0.15	4.06	2.33	0.88	119	47	0.18	6.55	18	34	38	111	24	166	155	33	181	18	1	5	671	65	55	53	15	3.29
MDZ113	1.78	1.70	14.55	68.42	0.14	3.52	1.19	0.75	96	45	0.14	4.97	17	21	25	83	20	148	138	29	203	14	1	6	616	68	212	50	14	1.28
MDZ135	2.41	2.91	16.00	63.11	0.20	3.58	4.87	0.58	74	32	0.11	5.13	16	16	24	84	23	190	393	47	198	18	1	6	504	78	132	22	18	0.96
MDZ136	2.47	2.96	15.72	62.66	0.22	3.42	4.29	0.64	79	27	0.12	5.36	19	17	24	86	22	168	389	40	229	17	1	5	480	72	300	20	17	1.16
MDZ140	0.82	1.95	20.04	62.84	0.15	3.18	1.19	0.93	128	56	0.09	6.74	20	31	53	124	28	166	144	33	211	18	2	6	911	78	67	44	20	0.96
MDZ149	2.00	2.94	17.46	59.87	0.18	3.41	4.98	0.82	138	49	0.11	6.96	21	30	37	111	23	137	322	32	193	13	2	4	739	81	32	24	14	0.50
MDZ150	1.33	3.05	19.09	56.09	0.21	4.11	5.34	0.90	156	75	0.11	8.66	23	43	43	132	27	163	206	37	156	15	1	5	893	88	53	22	15	0.40
MDZ151	1.58	2.92	15.37	64.60	0.23	2.98	2.86	0.89	116	60	0.15	6.70	24	34	40	155	21	118	229	31	228	13	2	5	586	67	220	34	14	1.23

Table 2 Elemental concentrations determined for the 88 individuals in this study. Major and minor elements are expressed as oxides in $w\%$. Trace elements are expressed in w mg/kg and loss on ignition (LOI) is expressed in $w\%$

Moreover, the compositional evenness graph (Fig. 3), inspired by the rank/abundance graph used in biodiversity studies (see, for example, Magurran 2004), examines the variability associated with each retained component. When all components contribute equal variability, evenness is maximised, and the information entropy (H_2), or Shannon index, attains its maximum value (the base-two logarithm of the number of components) (Buxeda and Madrid 2017; Shannon 1948). The assessment of compositional evenness, measured in decreasing order, is based on τ_j values (the sum of the variances following alr transformation using element j as a divisor). Greater dominance of variability by a few or a single component results in a significant decline in information entropy. The compositional evenness graph reveals that most of the variability is linked to the relative concentrations of Na_2O , Ni, Cr, Sr, and especially CaO (for these components, $tv/\tau_j < 0.5$), while Al_2O_3 and Ga ($tv/\tau_j > 0.9$) are the most stable components. Information entropy accounts for over 80% of the total attainable value ($H_2\% = 81.2$; $H_2 = 3.62$ Sh), indicating a chemical variability linked to numerous components. Both total variation and evenness serve as indicators of a complex structure within the data set.

CWA Provincial Inca pottery (n = 88)

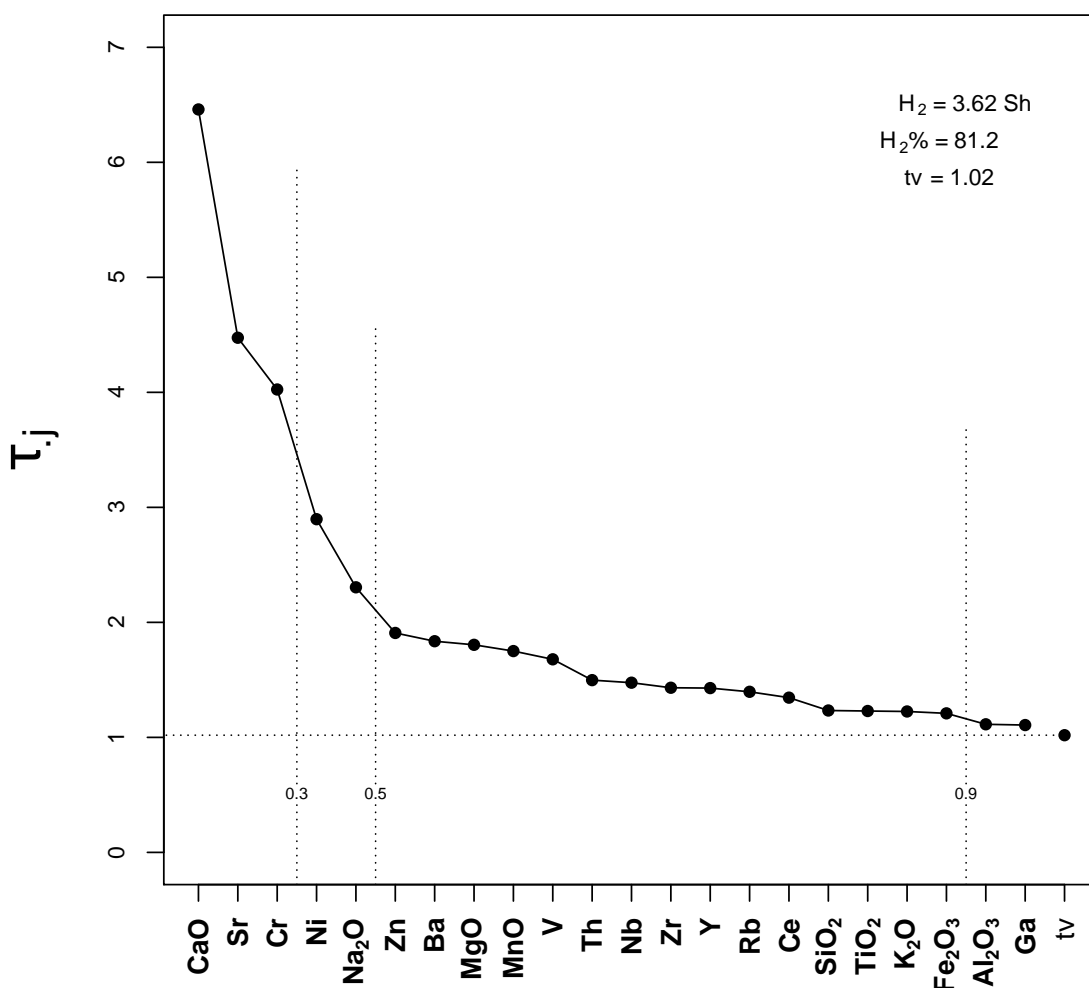


Fig. 3 Compositional evenness graph of the 88 individuals sampled. H_2 : information entropy (in shanons, Sh); $H_2\%$: percentage of the maximum possible attainable; tv : total variation; τ_j : sum of the variances following the alr transformation using element j as the divisor. Vertical dotted lines express different tv/τ_j values

Cluster analysis was performed using the squared Euclidean distance and agglomerative centroid algorithm on the clr-transformed retained components (Equation 2) (for the election of distance and agglomerative algorithm, see Buxeda 1999). Examination of the dendrogram (Fig. 4) enables us to propose the existence of a complex structure comprising six meaningful ceramic groups (or paste

compositional reference units, PCRU), each defined as a cluster containing three or more individuals. Additionally, fifteen individuals cannot be assigned to any group due to their compositional uniqueness. Nevertheless, individuals MDZ070 and 71 (indicated by arrows in Fig. 4) exhibit a close compositional similarity, but have not been considered a group. Notice that in the hierarchical cluster analysis of Figure 4, there is a node inversion, which can occur when using the centroid algorithm (Sneath and Sokal 1973; Manning et al. 2008, chapter 17). The six groups (Table 3) have been labelled from bottom to top in the order they appear in the dendrogram. Groups CGI02 and CGI03 are far more homogeneous than the rest. The experimental ceramic from Ranchillos (MDZ140, marked with a triangle) and the firing structure from RT285 (MDZ150, marked with an inverted triangle) are not clustered within any defined groups; they are placed on the bottom side of the dendrogram. Contrariwise, the experimental ceramic from RT285 (MDZ149, marked with a triangle) is situated within the CGI05 group.

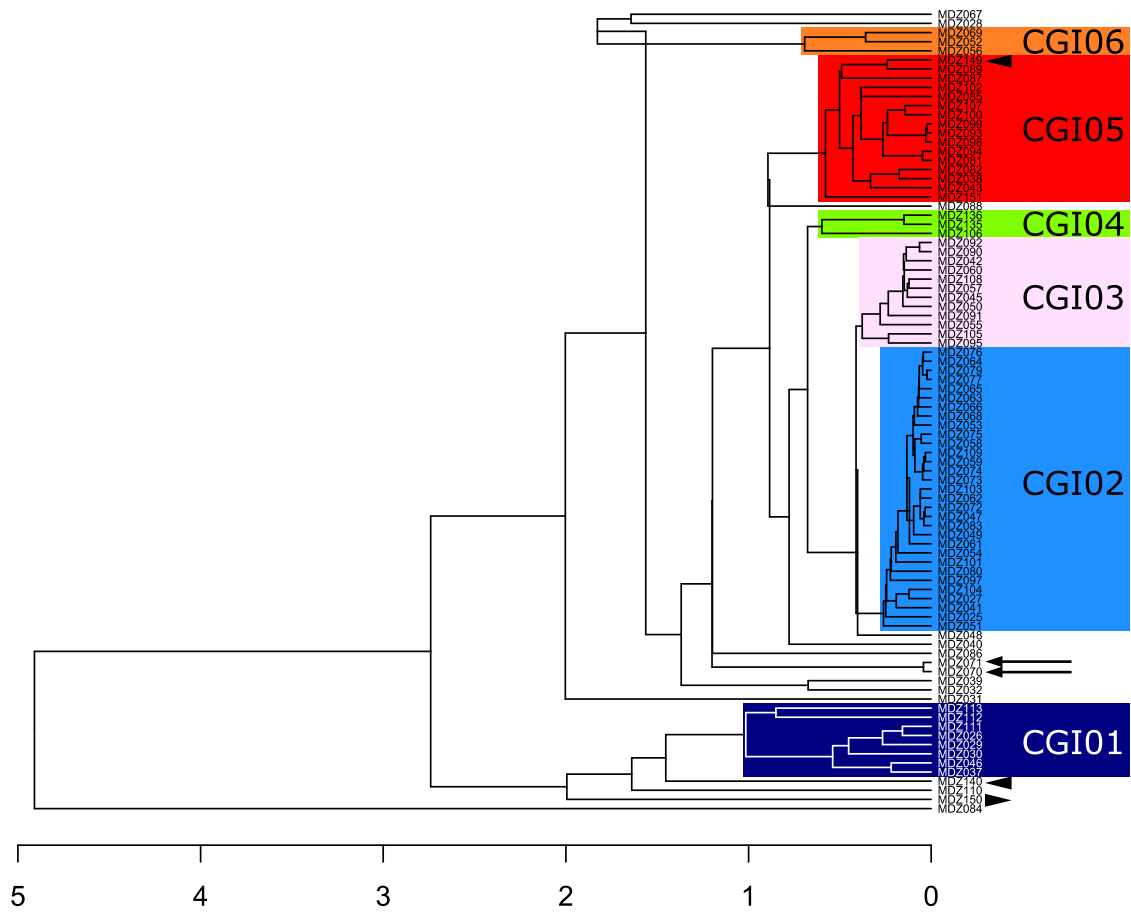


Fig. 4 Dendrogram from the cluster analysis performed using the squared Euclidean distance and the agglomerative centroid algorithm on the clr-transformed subcomposition Na₂O, MgO, Al₂O₃, SiO₂, K₂O, CaO, TiO₂, V, Cr, MnO, Fe₂O₃, Ni, Zn, Ga, Rb, Sr, Y, Zr, Nb, Ba, Ce and Th. Triangle: experimental ceramic. Inverted triangle: firing structure.

	CGI01 (<i>n</i> = 8) (<i>tv</i> = 0.48)		CGI02-Tambillos (<i>n</i> = 31) (<i>tv</i> = 0.14)		CGI03 (<i>n</i> = 12) (<i>tv</i> = 0.18)		CGI04 (<i>n</i> = 3) (<i>tv</i> = 0.24)		CGI05-RT285 (<i>n</i> = 16) (<i>tv</i> = 0.34)		CGI06 (<i>n</i> = 3) (<i>tv</i> = 0.33)	
	\bar{X}	<i>s</i>	\bar{X}	<i>s</i>	\bar{X}	<i>s</i>	\bar{X}	<i>s</i>	\bar{X}	<i>s</i>	\bar{X}	<i>s</i>
Na ₂ O	1.86	0.22	2.36	0.20	2.54	0.26	2.63	0.27	2.05	0.36	2.28	0.25
MgO	2.52	0.38	3.31	0.24	3.14	0.34	2.84	0.25	3.16	0.30	1.77	0.16

Al ₂ O ₃	18.44	1.54	16.56	0.32	16.79	0.60	16.07	0.12	17.57	1.00	17.17	1.22
SiO ₂	63.49	3.07	62.27	0.90	63.44	1.40	64.37	0.73	61.30	2.27	66.95	1.30
K ₂ O	3.91	0.29	3.44	0.22	3.49	0.31	3.59	0.09	3.61	0.27	3.73	0.30
CaO	1.77	0.68	5.14	0.67	3.39	0.64	4.28	0.70	4.16	1.26	1.82	0.19
TiO ₂	0.84	0.04	0.68	0.02	0.70	0.04	0.60	0.04	0.78	0.06	0.65	0.03
V	140	21	94	5	100	10	76	5	123	13	92	6
Cr	61	11	25	5	26	5	29	3	49	8	21	5
MnO	0.15	0.02	0.13	0.01	0.13	0.01	0.13	0.02	0.13	0.02	0.07	0.02
Fe ₂ O ₃	6.83	0.75	5.94	0.20	6.23	0.61	5.32	0.15	7.07	0.54	5.37	0.52
Ni	42	11	18	2	20	3	16	1	29	4	12	2
Zn	174	53	98	8	109	10	95	14	124	16	125	28
Ga	26	2	22	1	23	2	22	1	25	2	23	3
Rb	158	10	130	11	132	16	175	15	141	14	138	17
Sr	212	48	423	54	267	29	363	60	250	73	244	38
Y	33	2	32	2	32	2	43	4	34	2	36	3
Zr	186	14	202	9	195	10	237	39	192	16	222	13
Nb	14	2	12	1	12	1	17	1	13	1	13	1
Ba	820	140	585	66	554	39	491	20	624	81	793	134
Ce	71	2	72	5	73	7	80	7	78	7	81	5
Th	14	1	14	1	13	1	20	5	14	1	15	1

Table 3. Mean (\bar{X}) and standard deviation (s) of the defined groups on normalised data. *tv*: total variation. Major and minor elements are expressed as oxides in *w*%. Trace elements are expressed in *w* mg/kg

The relationships between the individuals and the retained components are clearly evident in the form and covariance biplots resulting from the singular value decomposition of the double-centred clr-transformed data (Fig. 5, top, left and right) (Aitchison and Greenacre 2002; Greenacre 2010; van de Boogaart and Tolosana-Delgado 2013). The form biplot shows the individuals in principal coordinates, giving a good approximation of the existing distances among them. In contrast, the arrows representing the components in standard coordinates tend to be spherical. This situation is reversed in the covariance biplot, where the arrows of the components are expressed in principal coordinates, optimally reflecting the covariance matrix, while the individuals are represented in standard coordinates, having their distances somehow distorted. Both biplots display the 0.95 probabilistic ellipsoids for groups containing more than 3 individuals. The form and covariance biplots resulting from the first two principal components explain almost 70% of the variance (VE = 69.15%).

In the form biplot (Fig. 5, top left), the existence of different groups, not necessarily located far from one another, and of ungrouped individuals is evident. The latter are scattered among the defined groups, but also positioned at greater distances from the centre of the biplot, showing more

pronounced differences in chemical composition. The covariance biplot (Fig. 5, top right) similarly highlights that the most significant contribution corresponds, as expected, to the double-centred clr-transformed components Cr, Ni, CaO, Sr and Na₂O, whose arrowheads lie far away from the centre. Cr (and Ni) versus Na₂O link on the same line but in opposite directions showing an inverse correlation, while CaO (and Sr) appear nearly orthogonal to this opposition. These patterns distinguish groups CGI05 and CGI01, ordered according to their relative content of CaO (and Sr), with higher relative values of Cr and Ni and lower relative values of Na₂O compared to groups CGI02, CGI04, CGI03 and CGI06 (Table 3).

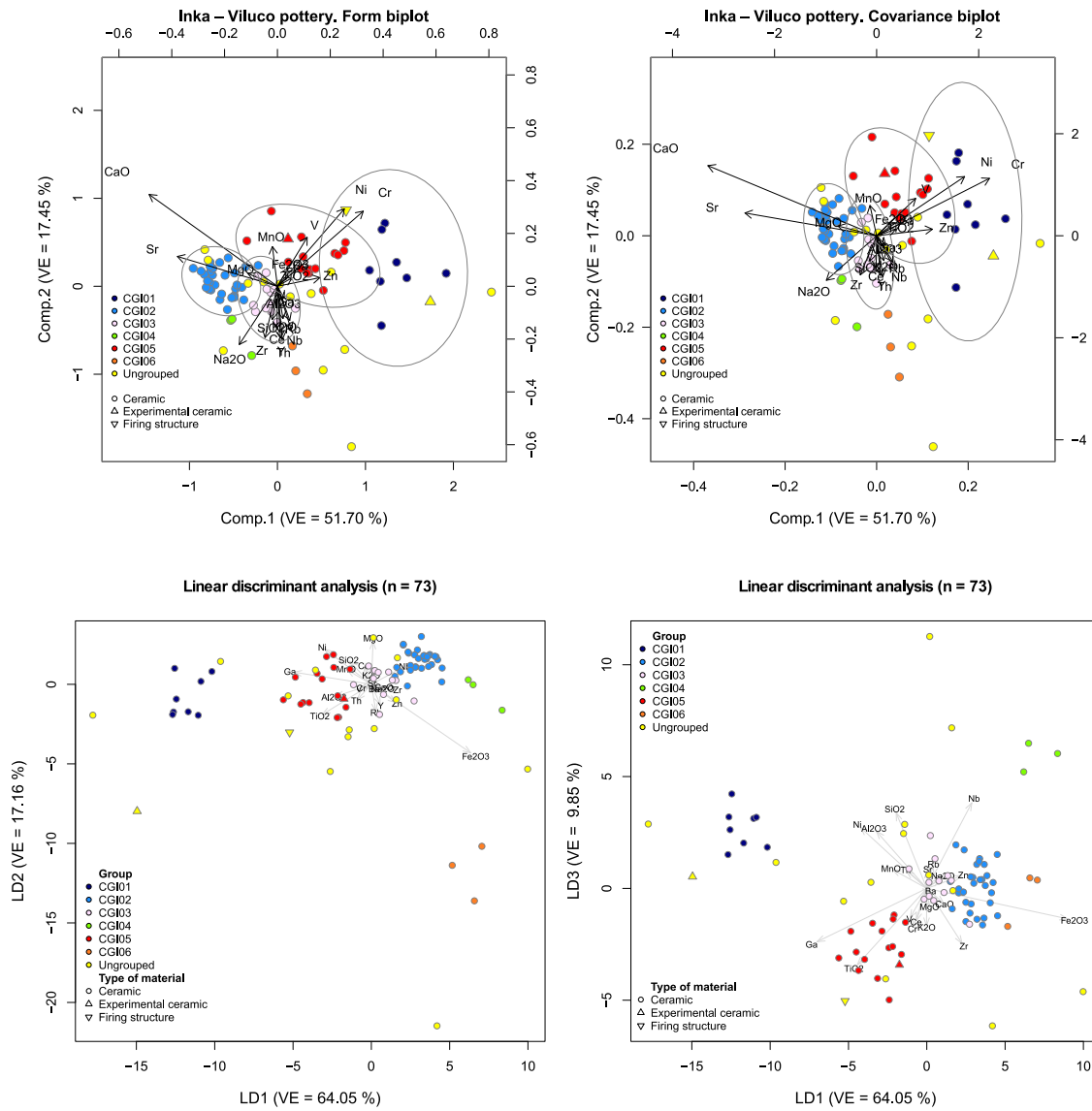


Fig. 5 Top: Biplots of the singular value decomposition on the double-centred clr-transformed subcomposition Na_2O , MgO , Al_2O_3 , SiO_2 , K_2O , CaO , TiO_2 , V , Cr , MnO , Fe_2O_3 , Ni , Zn , Ga , Rb , Sr , Y , Zr , Nb , Ba , Ce and Th . Probabilistic ellipses are shown for groups with more than 3 individuals ($p = 0.95$). **Left:** form biplot. **Right:** covariance biplot. **Bottom left:** Bivariate plot of the two first linear discriminants (LD) for the six defined groups, with the unstandardised coefficients and ungrouped individuals projected. VE: between-group variance explained. **Bottom right:** Bivariate plot of the first and third linear discriminants (LD) for the six defined groups, with the unstandardised coefficients and ungrouped individuals projected. VE: between-group variance explained

The linear discriminant analysis has further explored the consistency of the defined groups. Only the individuals in the six defined groups have been considered using the previously established subcomposition of retained components. The new variation matrix for the 73 individuals under consideration shows a noticeable decrease in total variation (from 1.02 to 0.78) and compositional evenness (from 81.2% to 78.7%), although most of the variability remains linked to the same components.

The linear discriminant analysis is thus conducted on the clr-transformed values of the six defined groups and plotting the first three linear discriminants. Subsequently, the ungrouped individuals are mapped onto the same plot using their clr-transformed values. Moreover, the unstandardised coefficients of the discriminant functions are also displayed. The plot with the first and second linear discriminants accounts for 81.21% of the variance observed between the groups in the 73 individuals (Fig. 5, bottom left), while the plot with the first and third linear discriminants accounts for 73.90% (Fig. 5, right). Thus, the first three linear discriminants account for 91.06% of the between-group variance. Displaying the unstandardized coefficients of the linear discriminants, it is also possible to observe the role played by Fe_2O_3 in the first linear discriminant, together with Ga, TiO_2 and Ni, while the second is dominated by MgO and Ni together with Fe_2O_3 , and the third one by Nb, SiO_2 , Ni and Al_2O_3 with TiO_2 , Ga and Zr. Table 3 shows that CGI04 and CGI06 exhibit a lower content of Fe_2O_3 , while CGI01 exhibits higher TiO_2 , Ni and MgO content. Notably, while certain groups are clearly discernible, groups CGI02 and CGI03 appear relatively close. Furthermore, the linear discriminant analysis classification table designates individual MDZ049, originally grouped in CGI02, as belonging to CGI03. Despite this possibility, the defined groups maintain a high degree of consistency.

Excluding the firing structure and experimental ceramics from consideration, the statistical treatment of the chemical data has enabled us to define six groups with clear compositional differences. Additionally, thirteen individuals (*ca.* 15%) remain ungrouped (although individuals MDZ070 and 71 could also be considered a new group on their own). These differences may correspond to as many as 18 different chemical compositions within the studied sample, which indicates a complex structure in CWA Inca provincial pottery production and distribution for the area under study. However, owing to this high complexity and the absence of significant chemical differences (as inferred from the total variation), this structure is not always clear-cut, and the final interpretation of the possible chemical groups is also strongly based on the mineralogical and archaeological pieces of evidence, and the petrographic information supplied by previous work (Carosio and Ots 2022) that will be explained below. To some extent, more individuals must be characterised to deepen our present knowledge. In

this context, since the sample includes too many sites —eleven (excluding Ranchillos, which only contributes the experimental ceramic MDZ140)— and four types of pottery for only 85 archaeological ceramics, the inferences that can be drawn are necessarily weak. Nevertheless, some points still warrant emphasis.

A summary of the current results is presented (Table 4), featuring a frequency table of the retrieval site and group. The last column (ungrouped) logically differs from the previous ones because the individuals listed there are not necessarily part of the same meaningful chemical group. Furthermore, the retrieval site is hierarchically organised, with a first level corresponding to the broad retrieval areas (Uco Valley, Uspallata Valley, and the foothills and plains of south San Juan province). Even if the frequencies are too low with several expected frequencies falling below 5, the χ^2 test shows no significant differences for the 85 samples between the frequencies of grouped and ungrouped individuals across these 11 sites ($\chi^2 (10, n = 85) = 8.21, p = 0.61$). This first result suggests that less common products are similar across all the sites considered. Even so, the distribution of the groups in the three broad areas seems uneven.

Area	Site	CGI01	CGI02	CGI03	CGI04	CGI05	CGI06	Ungrouped	Total
Uco valley	Agua Amarga	7	3	2		3		5	20
	Atamisque	1						1	2
Uspallata valley	Potrero Chanchería		7	4			2	1	14
	Tambillos (I. s.) (p. c.)		9	1			1	1	12
	Ciénaga Yalguaraz (I. s.)		2					2	4
	Ranchillos (I. s.)							1	1
	Tambillitos (I. s.)		5						5
Foothills south San Juan province	Altos de Melián			1		2		1	4
	RT285 (p. c.)		2	2		6		1	11
	El Pozo		2			1		1	4
	Arroyo Cieneguita			1		1			2
	Retamito		1	1	3	3		1	9
Total		8	31	12	3	16	3	15	88

Table 4 Frequency table of retrieval site and chemical group. (I. s.): Inka site; (p. c.): production centre

Group CGI01 is only found in Uco Valley, while almost all ceramics belonging to group CGI05 are found in the foothills of south San Juan province (except for three individuals retrieved from Agua

Amarga). At the same time, both CGI01 and CGI05 are absent in Uspallata Valley. Contrariwise, the main groups present at the sites of Uspallata Valley, CGI02 and CGI03, are also prevalent in Uco Valley and the foothills of south San Juan province. The other two small groups, namely CGI04 and CGI06, with only three individuals each, are found in the foothills of south San Juan province (at Retamito) and Uspallata Valley, respectively. This distribution pattern suggests the existence of local groups in Uco Valley (CGI01) and the foothills of south San Juan province (CGI05 and CGI04) that are absent in Uspallata Valley. Conversely, certain groups identified in Uspallata Valley (CGI02 and CGI03) are also found in the other two areas, indicating a broader regional distribution for these particular groups.

The final important point is that CGI02 is especially present at Tambillos, while the same happens at RT285 with CGI05. These findings could support the identification of both sites as production centres. By excluding groups CGI04 and CGI06 due to their low frequencies, the χ^2 test confirms the previous association between areas and groups ($\chi^2 (6, n = 67) = 54.65, p \approx 0$). The contributions to the χ^2 exhibit clear associations for all groups except CGI03, which shows a close agreement between observed and expected frequencies across the three areas.

Even though the frequencies are low, the correspondence analysis between groups and sites reveals a general structure with three different trends. The analysis of the six groups and a group of ungrouped individuals accounts for the first three linear discriminants, explaining up to 85.9% of the inertia (Fig. 6, A and B). The first two dimensions (Fig. 6, A) show the two sites from Uco Valley to the far positive site of dimension 2, attracted by CGI01; the sites from the foothills and plains of south San Juan to its negative side, attracted by CGI05 and CGI04; and the sites from Uspallata Valley to the positive side of dimension 1, attracted by CGI02 and CGI06. Group CGI03 and the ungrouped individuals remain at the centre, as they are evenly distributed across all sites. Only two sites show slightly different behaviour. On the one hand, El Pozo is closer to the Uspallata Valley trend because half of its assemblage belongs to group CGI02 (2 out of 4; 1 belongs to CGI05; and 1 is ungrouped). On the other hand, Ciénaga Yalguaraz stands apart from the Uspallata trend and is closely aligned with the ungrouped category, as 2 out of 4 individuals are ungrouped (the remaining two belong to CGI02). The first and third dimensions show a clear difference between Retamito and all other sites from the foothills and plains of south San Juan because all 3 individuals of group CGI04 were recovered at this site. Upon repeating this analysis while excluding ungrouped individuals (Fig. 6, C and D) (90.6% of inertia), the structure remains consistent. However, Ciénaga Yalguaraz is now clearly placed within the Uspallata Valley trend, while El Pozo exhibits a strong attraction to this trend, occupying an intermediate position.

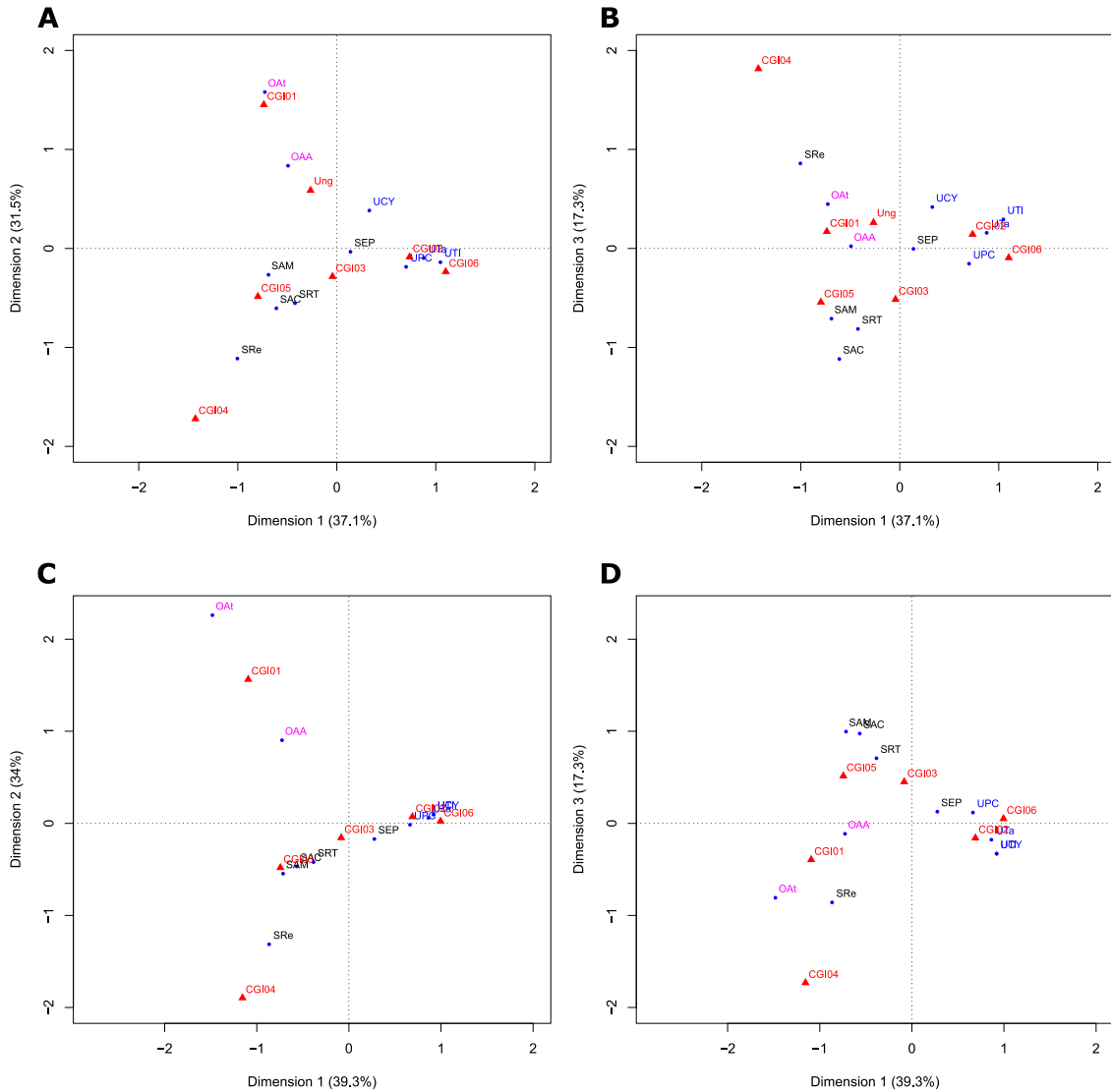


Fig. 6 Biplot of the correspondence analysis of the 85 archaeological ceramics by group and site. **A**: dimensions 1 and 2, with the six groups and a group of ungrouped individuals. **B**: dimensions 1 and 3, with the six groups and a group of ungrouped individuals. **C**: dimensions 1 and 2, with the six groups, without a group of ungrouped individuals. **D**: dimensions 1 and 3, with the six groups, without a group of ungrouped individuals. Red dots: groups. Blue dots: sites (magenta labels: Uco Valley; blue labels: Uspallata Valley; black labels: foothills and plains of south San Juan province). OAA: Agua Amarga, OAt: Atamisque, UPC: Potrero Chanchería, UTa: Tambillos, UCY: Ciénaga Yalguaraz, UTI: Tambillitos, SAM: Altos de Melián, SRT: RT285, SEP: El Pozo, SAC: Arroyo Cieneguita, SRe: Retamito.

The association of the chemical groups with a presumed area of provenance is strengthened by comparing these results with the petrofabrics (PF) defined in the petrographic analysis of 24 of these individuals, carried out by Carosio and Ots (2022) (Table 1). The trend is clear in certain instances. All individuals from CGI02, except for one (MDZ061, PF1), were grouped under PF4 (MDZ066, 68, 73, 76, 79), and those from CGI06 were categorised within PF8 (MDZ052, 69). Both petrofabrics are characterised by a high presence of volcanic and metamorphic rocks, grog, and plutonic rocks in PF8. This composition is typical of the volcanic geological context of Uspallata Valley (Choiyoi group in the Cordillera frontal). PF2 includes two individuals grouped under CGI04 (MDZ106, 136) from Retamito, while PF6 is mainly composed of samples grouped within CGI05 (MDZ081, 82, 85, 87, 93, 100). Both petrofabrics could be located in southern San Juan production areas due to their geological composition (volcanic rocks, granites, granitoid, metamorphic rocks and metamorphosed felsic minerals). However, PF2 lacks the sedimentary rocks abundant in the foothill deposits and alluvial plain of the rivers that originate in Cordillera Frontal and Precordillera.

Finally, the two individuals from group CGI01 that underwent petrographic analysis were classified in PF1 (MDZ046) and PF5 (MDZ112). The frequency distinguishes these PFs in terms of the composition of felsic and intermediate volcanic rocks with aphanitic and devitrification texture, felsic minerals, sedimentary rocks, and low proportions of oxide and opaque minerals. In PF1, grog, biotite, muscovite, amphibole and pyroxene are also present. The association of these with the geology of Uspallata Valley (PF1) and southern San Juan (PF5), respectively, is probable (Carosio and Ots 2022). Lastly, CGI03 comprises samples described in PF1 (MDZ050, 60), PF4 (MDZ57) and PF6 (MDZ091, 92, 105). The partial correspondence between chemical groups and petrofabrics underscores the challenges inherent in interpreting data in such a complex and somewhat similar environment. Nevertheless, the association between groups CGI02 and CGI06 with petrofabrics PF4 and PF8, related to Uspallata Valley, and groups CGI03 and CGI05 with petrofabrics PF2 and PF6, linked to southern San Juan, remains evident.

Shifting our focus to the types of pottery under study (Table 5), the comparison between grouped and ungrouped individuals reveals no discernible association (χ^2 (3, n = 85) = 3.09, p = 0.38). A first glance at Table 5 indicates that groups CGI02 and CGI03 include all different pottery types, including fine, ceremonial vessels and utilitarian wares. However, the χ^2 test confirms an association between types and groups (χ^2 (9, n = 67) = 23.80, p = 0.004), mainly attributed to the great number of *ollas* in group CGI05 and store jars in CGI02. Other minor, yet significant, contributions arise from the absence of *ollas* in CGI01, storage jars in CGI4 and CGI6, and the elevated count of *urpu* within

group CGI02. After all, 17 out of the 30 *ollas* were sampled from the foothills and plains of south San Juan province, and an equivalent number of storage jars were recovered from Uspallata Valley (Table 1). Therefore, considering the distribution of types in the areas under study (Table 1), it becomes evident that not only *ollas* but also storage jars are unevenly represented in different areas (χ^2 (6, n = 85) = 13.75, p = 0.03). However, interpreting this association is difficult due to the uneven distribution of pottery types within each area. The divergent social and economic dynamics of local and Inca sites imply variability in the ceramic assemblages, which is reflected in the products of each chemical group.

Ceramic type	Form	CGI01	CGI02	CGI03	CGI04	CGI05	CGI06	Ungrouped	Total
Fine or ceremonial vessels	<i>Aryballo or urpu</i>	4	8	2	1	1		2	18
	<i>Puco</i>	1	2	2	1		1		7
	<i>Olla</i>		5	4	1	11	2	7	30
Utilitarian vessels	Storage jar	3	16	4		3		4	30
Comparative samples	Experimental ceramics					1		1	2
	Firing structures							1	1
Total		8	31	12	3	16	3	15	88

Table 5 Frequency table of ceramic type and chemical group

4. 2. Mineralogical and microstructural characterisation

The chemical results reveal that all analysed individuals correspond to ceramics technically classified as low calcareous (CaO < 5%-6%), except for group CGI02, which corresponds to border calcareous ceramics (*ca.* 5% < CaO < 6%). Regarding phase transformations –*i.e.*, decomposition of primary phases and crystallisation of firing ones, as well as densification during firing through sintering and, possibly, vitrification, inducing microstructural changes (Heimann and Maggetti 2014; Maggetti 1981; Maniatis and Tite 1981; Maniatis et al. 1981; Tite et al. 1982), low calcareous ceramics develop fewer high-temperature phases than calcareous pottery. Additionally, they develop a denser microstructure with a rapid formation of a vitreous phase.

As illustrated in the ternary phase diagram CaO-Al₂O₃-SiO₂ (Fig. 7, A), all groups fall within the anorthite-mullite-quartz thermodynamic equilibrium triangle due to their low calcareous composition. Thermodynamic considerations suggest that these mineralogical phases should be the final phases present at high temperatures. Nevertheless, this system does not consider kinetics and represents a simplification of actual composition. In most cases, such as this, mullite does not

crystallise as a firing phase. Instead, spinel is found when magnesium is present in noticeable concentrations (typically $MgO > 1\%$) (Table 2).

Group CGI02, the border-calcareous one, and two individuals belonging to group CGI05 are situated closer to the boundary with the quartz-anorthite-wollastonite triangle, characteristic of calcareous ceramics. These two individuals (MDZ087 and 89) display higher CaO content than the rest of the CGI05 group. Such ceramics sometimes exhibit behaviour similar to calcareous ceramics and can even contain pyroxene as a firing phase.

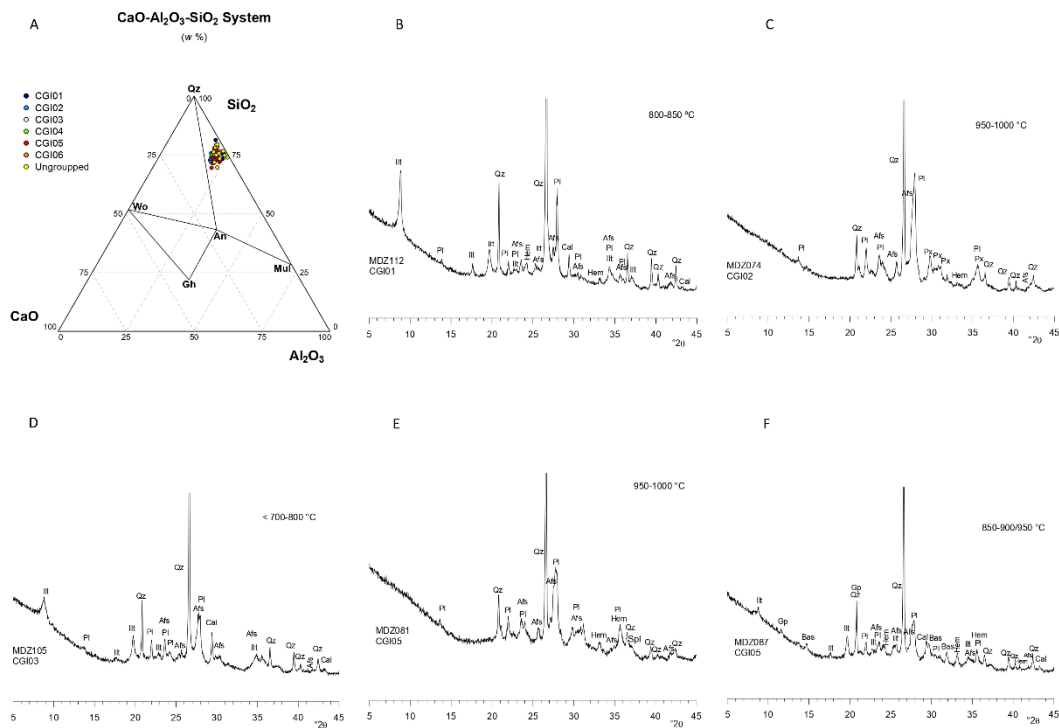


Fig. 7 A: Phase diagram of the ternary system $CaO-Al_2O_3-SiO_2$ showing the situation of the individuals analysed. An: anorthite ($Ca[Al_2Si_2O_8]$), Gh: gehlenite ($Ca_2Al(Si,Al)_2O_7$), Mul: mullite ($Al_6[Si_2O_{13}]$), Qz: quartz (SiO_2), Wo: wollastonite ($CaSiO_3$). **B:** Diffractogram of individual MDZ112, fabric F1, group CGI01. **C:** Diffractogram of individual MDZ074, fabric F3, group CGI02. **D:** Diffractogram of individual MDZ105, fabric F1, group CGI03. **E:** Diffractogram of individual MDZ081, fabric F4, group CGI05. **F:** Diffractogram of individual MDZ087, fabric F5, group CGI05. Afs: alkali feldspar, Bas*: bassanite, Cal: calcite, Gp: gypsum, Hem: hematite, Ill: illite-muscovite,

Pl: plagioclase, Px*: pyroxene, Qz: quartz, Spl: spinel (abbreviations according to Whitney and Evans, 2010, except for * bassanite and pyroxene)

Mineralogical and microstructural changes enable estimating the equivalent firing temperature (EFT) of archaeological ceramics (Roberts 1963) by comparing them with controlled experiments. In the present study, two experiments were conducted on individuals MDZ140 and MDZ149 to estimate the EFT (Ots and Cahiza 2016). Furthermore, the knowledge derived from other experiments involving ceramics and clays of a similar composition provides supplementary information regarding the general trend of changes undergone by different types of pottery under different firing conditions (Buxeda et al. 2002; Heimann and Maggetti 2014; Madrid 2006; Maggetti 1981, 1982; Maniatis and Tite 1978; Maniatis et al. 1981, 1983; Tsantini et al. 2004).

The study of XRD diffractograms of the individuals within CGI01 allowed the identification of two fabrics (F1 and F2), which represent different categories of crystalline phase association (Table 6). Both fabrics present alkali feldspar, plagioclase, quartz, hematite and illite-muscovite, but only F1 contains calcite (Fig. 7, B). The origin of calcite in fabric F1 remains uncertain. It could correspond to primary calcite not decomposing during firing. The decomposition of calcium carbonate starts above 550 °C depending on the equilibrium CO₂ pressure in the air, among other significant variables (*i.e.*, Rodriguez-Navarro et al. 2009). In ceramics, primary calcite usually decomposes above 700 °C or 800 °C, and it is still found even at higher temperatures when coarse limestone grains are present (Buxeda and Cau 1995; Cau et al. 2002; Fabbri et al. 2014). Alternatively, it might have a secondary origin (*i.e.*, crystallised after firing), but still, there is insufficient evidence.

In any case, the CaO content of this individual falls well within the concentrations of group GCI01, and the presence of calcite cannot be used to infer the EFT. Moreover, while hematite could exist as a primary phase, its formation can also occur through the crystallisation of iron hydroxides at 400 °C, or the dehydroxylation of clay minerals. Under such circumstances, experimental firing can identify hematite above 800 °C or 850 °C. However, since hematite is observed in all individuals, its presence also fails to provide indications to estimate the EFT. Therefore, the only sound mineralogical evidence is the existence of illite-muscovite that is usually present in EFT up to 950 °C-1000 °C. This observation points clearly to an EFT below this range, potentially even below 950 °C, due to the absence of firing phases. The SEM study could help narrow down this range after microstructural changes during densification. Unfortunately, only one group member remained extant and available for sampling. Thus, individual MDZ112 (F1) exhibits a microstructure characteristic of the sintering

stage of initial vitrification (IV), with the first formation of isolated smooth-surfaced areas (Fig. 8, A), which enables to estimate an EFT in the range of 800 °C to 850 °C.

XRD fabric	Mineral phases	Individuals	Sintering stage	EFT °C
CGI01 (n = 8)				
F1 (n = 1)	Qz, Ilt, Afs, Hem, Pl, Cal	MDZ112 ^{SEM}	IV	800-850
F2 (n = 7)	Qz, Ilt, Afs, Hem, Pl	MDZ026, 29, 30, 37, 46, 111 and 113	n.d.	< 950-1000 (< 900-950 ?)
CGI02 (n = 31)				
F1 (n = 3)	Qz, Ilt, Afs, Hem, Pl, Cal	MDZ066 ^{SEM} , 97 and 103	NV	< 800
F2 (n = 22)	Qz, Ilt, Afs, Hem, Pl, Px*	MDZ025, 27, 47, 49, 53, 54, 58, 59, 62 ^{SEM} , 63, 64, 65, 68, 72, 73, 75, 77, 79 ^{SEM} , 80, 83, 101 and 104	NV-V	ca. 800-850/950
F3 (n = 6)	Qz, Afs, Hem, Pl, Px*	MDZ041, 51, 61, 74 ^{SEM} , 76 and 109	V + FH	950-1000
CGI03 (n = 12)				
F1 (n = 1)	Qz, Ilt, Afs, Pl, Cal	MDZ105 ^{SEM}	NV	< 700-800
F2 (n = 1)	Qz, Ilt, Afs, Pl	MDZ060 ^{SEM}	NV	< 800
F3 (n = 5)	Qz, Ilt, Afs, Pl, Hem	MDZ042, 50, 55, 92 and 95 ^{SEM}	IV	800-850
F4 (n = 5)	Qz, Afs, Pl, Hem (Ilt ?)	MDZ045, 57 ^{SEM} , 90, 91 ^{SEM} and 108	V-TV	850/950-950/1000
CGI04 (n = 3)				
F1 (n = 3)	Qz, Afs, Pl, Hem	MDZ106, 135 ^{SEM} and 136	TV	950-1000
CGI05 (n = 16)				
F1 (n = 1)	Qz, Ilt, Afs, Hem, Pl, Cal	MDZ100 ^{SEM}	IV	800-850
F2 (n = 7)	Qz, Ilt, Afs, Hem, Pl	MDZ043, 82 ^{SEM} , 85, 94, 107, 149 (e.c.) and 151	V	850-900/950
F3 (n = 3)	Qz, Ilt (not 10 Å peak), Afs, Hem, Pl, Spl	MDZ093, 98 and 99	n.d.	900/950-950/1000
F4 (n = 3)	Qz, Afs, Hem, Pl, Spl	MDZ038, 81 ^{SEM} and 102	TV + FH	950-1000
F5 (n = 1)	Qz, Ilt, Afs, Hem, Pl, Cal, Gp, Bas*	MDZ087 ^{SEM}	V	850-900/950
F6 (n = 1)	Qz, Ilt, Afs, Hem, Pl, Gp, Bas*	MDZ089	n.d.	850-900/950
CGI06 (n = 3)				
F1 (n = 2)	Qz, Ilt, Afs, Hem, Pl	MDZ052 and 56 ^{SEM}	NV-V (+ FH ?)	850-900/950
F2 (n = 1)	Qz, Afs, Hem, Pl, Spl	MDZ069 ^{SEM}	TV + FH	950-1000

Table 6. Summary of the mineralogical fabrics defined by PXRD and SEM analyses for each of the six chemical groups. Mineral phase names abbreviations: Afs: alkali feldspar, Bas*: bassanite, Cal: calcite, Gp: gypsum, Hem: hematite, Ilt: illite-muscovite, Pl: plagioclase, Px*: pyroxene, Qz: quartz, Spl: spinel (according to Whitney and Evans 2010, except for * bassanite and pyroxene). Sintering stages abbreviations: NV: no vitrification, IV: initial vitrification, V: extensive vitrification, TV: total vitrification, FH: fast heating. ^{SEM}: individual studied by SEM. e.c.: experimental ceramic

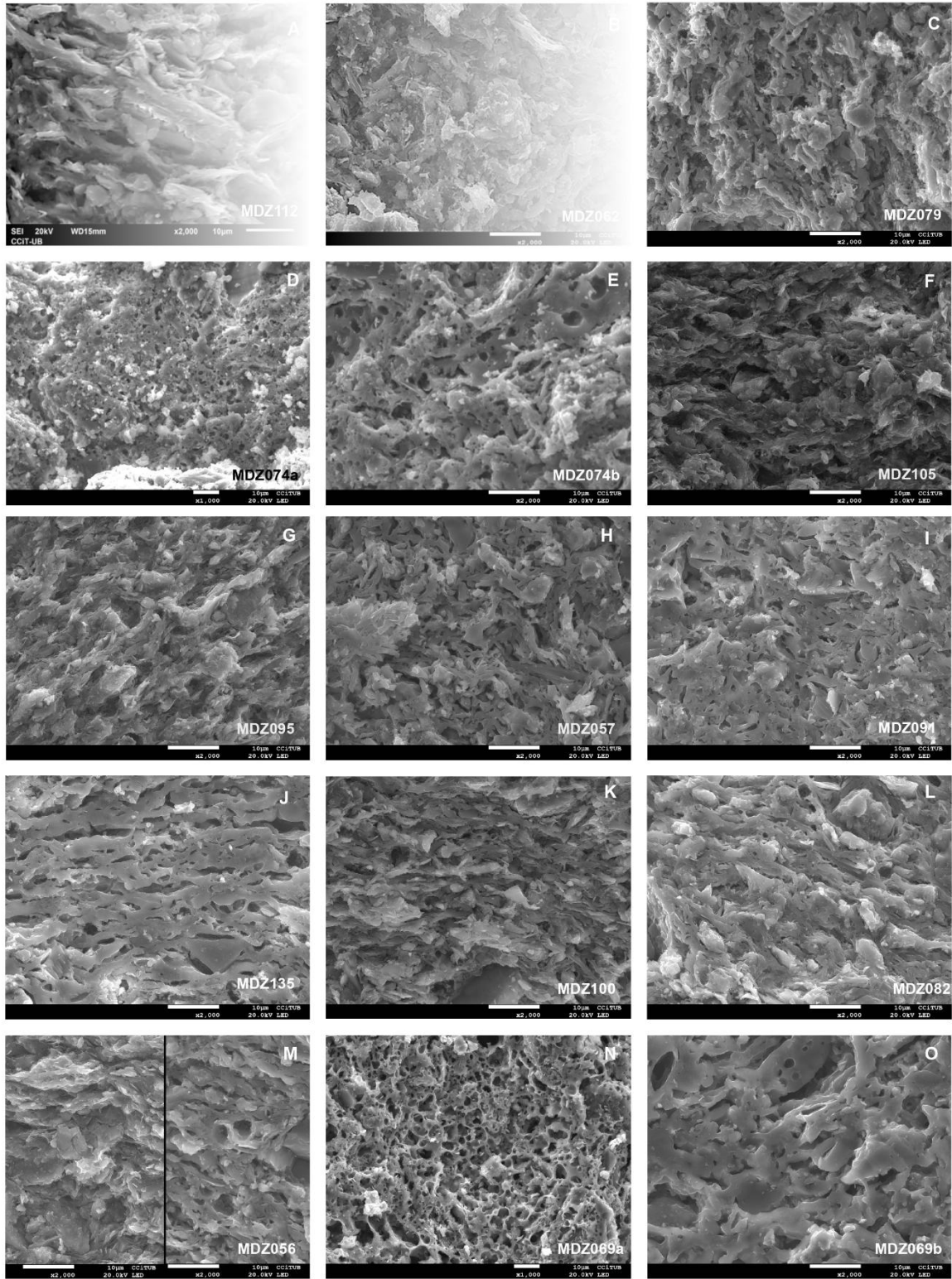


Fig. 8 SEM photomicrographs. **A:** MDZ112, fabric F1, group CGI01, IV. **B:** MDZ062, fabric F2, group CGI02, NV. **C:** MDZ079, fabric F2, group CGI02, V. **D:** MDZ074a, fabric F3, group CGI02,

fine bloating pores of fast heating. **E**: MDZ074b, fabric F3, group CGI02, V. **F**: MDZ105, fabric F1, group CGI03, NV. **G**: MDZ095, fabric F3, group CGI03, IV. **H**: MDZ057, fabric F4, group CGI03, V. **I**: MDZ091, fabric F4, group CGI03, TV. **J**: MDZ135, fabric F1, group CGI04, TV. **K**: MDZ100, fabric F1, CGI05, IV. **L**: MDZ082, fabric F2, group CGI05, V. **M**: MDZ056, fabric F1, group CGI06, (left) NV and (right) V. **N**: MDZ069a, fabric F2, group CGI06, fine bloating pores of fast heating. **O**: MDZ069b, fabric F2, group CGI06, TV. NV: no vitrification, IV: initial vitrification, V: extensive vitrification, TV: total vitrification.

The border calcareous group GCI02 contains three different fabrics (F1 to F3) (Table 6). Fabric F1 includes three individuals and exhibits alkali feldspar, plagioclase, quartz, hematite, calcite and illite-muscovite. In contrast with the previous group, the calcite observed in this fabric can be considered a primary phase since it is not present in the subsequent fabrics, implying a higher EFT. SEM analysis reveals a microstructure characterised by a sintering stage of no vitrification (NV). These observations allow us to estimate an EFT below 800 °C. The decomposition of this primary calcite would contribute to the crystallisation of pyroxene (possibly diopside) in fabric F2, as the EFT increases. In firing experiments, pyroxene crystallisation has been observed from 700 °C or 800 °C onwards, which coincides with the range where calcite decomposition usually occurs.

Within fabric F2, SEM examination shows differences between individual MDZ062 (Fig. 8, B), with no vitrification (NV), and MDZ079 (Fig. 8, C), with extensive vitrification (V). Therefore, the EFT for fabric F2 must be estimated between no vitrification (below 800 °C) and extensive vitrification (850 °C-950 °C). However, the lower end of the range must be close to 800 °C because calcite decomposition and pyroxene crystallisation have already occurred. Fabric F2 comprises a total of 22 individuals. Of these, individuals MDZ053, 68 and 101 exhibit an intermediate diffractogram between fabrics F1 and F2, with unclear pyroxene peaks, while individuals MDZ054, 58, 72, 73 and 75 show intermediate diffractograms between fabrics F2 and F3, with unclear illite-muscovite peaks.

The total decomposition of illite-muscovite defines fabric F3 (Fig. 7, C), which comprises 6 individuals. The microstructure here consists of a continuously vitrified surface containing a high concentration of fine bloating pores, with a small diameter typically below 5 µm (Fig. 8, D and E). This kind of microstructure is typically produced in a reducing atmosphere through fast heating, as seen in bonfires or pits where fuel and pots are in contact (Buxeda et al. 2003; Maniatis and Tite 1975, 1978; Maniatis and Tsirtsoni 2002). Furthermore, the colours exhibited by the vessels suggest that the post-firing cooling of these ceramics must have occurred in oxidising atmospheres. The extent of

reoxidation that masks the typical grey core colours associated with the bloating pore areas suggests that potters intentionally create an early oxidising atmosphere during the cooling process as soon as the firing is complete. Prior to overfiring the ceramic, the EFT must be estimated at 950 °C-1000 °C.

Regarding group CGI03, up to 4 fabrics have been defined by XRD (Table 6). The first one, F1, includes only the individual MDZ105. This fabric contains alkali feldspar, plagioclase, quartz, calcite and illite-muscovite, and the EFT can be estimated below 700 °C-800 °C due to the presence of calcite and the absence of hematite (Fig. 7, D). This estimation aligns with the no vitrification (NV) sintering stage, indicating an EFT below 800 °C (Fig. 8, F). Fabric F2 also includes a single individual (MDZ060). The only difference from the previous fabric is the absence of calcite, which is not observed. However, it shares similarities such as the absence of hematite and a sintering stage of no vitrification (NV). The estimated EFT is below 800 °C.

Fabric F3 accounts for five individuals. Their diffractograms show the presence of hematite, which must be considered a firing phase, indicating an EFT above 800 °C or 850 °C. Additionally, the presence of illite-muscovite provides an upper limit of 950 °C to 1000 °C. This range is consistent with the SEM observation of the microstructure in individual MDZ095, exhibiting initial vitrification (IV) (Fig. 8, G). Such a stage can be associated with an EFT of 800 °C to 850 °C.

Finally, fabric F4 also includes five individuals. The XRD results indicate that illite-muscovite is virtually decomposed, allowing for an EFT above 950 °C to 1000 °C or slightly below. No firing phases are observed. The microstructures observed by SEM show differences in the sintering stage, ranging from extensive vitrification (V) (Fig. 8, H) to total vitrification (TV) (Fig. 8, I). The first stage corresponds to an EFT in the range of 850 °C to 950 °C, while the second one corresponds to 950 °C to 1000 °C, just before overfiring.

The three individuals in group CGI04 share similar mineralogical and microstructural characteristics. The only fabric (F1) in this group displays alkali feldspar, plagioclase, quartz and hematite, while illite-muscovite is absent. The sintering stage is total vitrification (TV) (Fig. 8, J), allowing for an EFT in the range of 950 °C to 1000 °C (Table 6).

Group CGI05 presents a high diversity of fabrics defined through XRD analysis (Table 6). Individual MDZ100 constitutes fabric F1, exhibiting illite-muscovite, alkali feldspar, calcite, plagioclase, quartz and hematite, with a microstructure featuring an initial vitrification (IV) sintering stage (Fig. 8, K). EFT can be estimated at 800 °C-850 °C, suggesting a possible secondary origin for calcite. Fabric F2 closely resembles the previous one but lacks calcite. The microstructure (Fig. 8, L) shows extensive

vitrification (V), corresponding to an EFT at 850 °C-950 °C. The absence of spinel, however, implies a lower EFT in the range of 850 °C to 900 °C-950 °C. It must be highlighted that individual MDZ149 is an experimental sample fired at 900 °C (Ots and Cahiza 2016). The crystallisation of spinel as a firing phase defines the next fabric, F3. This phase typically forms at an EFT over 900 °C-950 °C. The near decomposition of illite-muscovite, with only an extant low-intensity peak at 4.5 Å, suggests an EFT at 950 °C-1000 °C. Finally, fabric F4 presents the highest EFT due to the decomposition of illite-muscovite (Fig. 7, E) and the development of a total vitrification (TV) sintering stage with the characteristic bloating pores resulting from fast heating. The mineral phases enable an EFT estimate over 950 °C-1000 °C, with the sintering stage occurring at 950 °C-1000 °C, just before overfiring.

The last two individuals in this group define a different fabric each, F5 and F6. The mineralogical phases and sintering stage are similar to fabric F2 but differ in the presence of secondary phases. In F5, these phases include gypsum, bassanite and calcite (Fig. 7, F). The latter is absent in F6. Gypsum ($\text{CaSO}_4 \cdot 2\text{H}_2\text{O}$) is a calcium sulphate dihydrate, while bassanite ($\text{CaSO}_4 \cdot 0.5\text{H}_2\text{O}$) is a calcium sulphate hemihydrate. Both individuals were recovered at Altos de Meli n, a site in Lagunas de Guanacache's arid area. Thus, in such conditions, gypsum and calcite might be clear authigenic minerals (Jafarzadeh and Burnham 1992). The presence of bassanite is likely a result of the specimens preparation process for XRF and XRD examination. It is well known that gypsum dehydrates in two different steps, first to hemihydrate and then to anhydrite (CaSO_4). The first step may result from the milling process (Zhang et al. 1996) and especially through heating at low temperatures in the range of 80 °C to 130 °C, depending on other relevant variables (Yu and Brouwers 2012), similar to those used during specimen drying in an oven. Along these lines, it is important to note that both individuals exhibit the highest CaO concentration in group CGI05, possibly pointing to a partial allochthonous origin of calcium due to these secondary mineral phase formations.

For the last group, CGI06, two distinct fabrics have been defined (Table 6). F1 exhibits illite-muscovite, alkali feldspar, plagioclase, quartz and hematite without firing phases. The microstructure, however, exhibits a particular sintering stage with clear differences between the core and the outer part of the matrix. The latter shows no vitrification (NV) (Fig. 8, M, left) in contrast with the core where extensive vitrification (V) is observed (Fig. 8, M, right). A similar difference between the core and the outer part is also present in fabric F2. In this case, bloating pores have entirely changed the microstructure of the core (Fig. 8, N), whereas the outer part shows total vitrification (TV) with few bloating pores (Fig. 8, O). Illite-muscovite in this fabric is decomposed, and spinel has formed as a firing phase. The contrast between the core and the outermost parts of the matrix is typically observed in instances of fast heating rates. However, within group CGI06, this discrepancy is noted at lower

EFT without bloating pores (Fig. 8, M). In summary, the EFT for F1 can be estimated in the range of 850 °C to 900 °C-950 °C, while for F2 it can be estimated at 950 °C-1000 °C, without overfiring.

Regarding the 15 non-classified individuals, the XRD results provide limited insight to estimate EFT because mineralogical scales can only be assumed within chemical groups showing different fabrics. Moreover, none of these individuals underwent SEM observations, as such results would solely pertain to the specific individual without the possibility of extending inferences to a fabric. However, some observations can be highlighted. All individuals exhibit the presence of hematite with different intensities, which aligns with the production of reddish pottery. If hematite is indicative of a firing phase, this implies an EFT above 800 °C or 850 °C. The only individual where illite-muscovite is not observed is MDZ028, an *olla* from Agua Amarga. This individual also displays the presence of spinel, which can most probably be identified as a firing phase, suggesting an EFT at 950 °C-1000 °C, just before overfiring.

Finally, individual MDZ084, an *aryballos* from Retamito, exhibits intense peaks of analcime, a sodic zeolite. Analcime has usually been observed as a secondary phase in non-severely overfired calcareous pottery (Buxeda 1999; Schwedt et al. 2006). However, in this case, with low calcareous pottery and intense illite-muscovite peaks, it is most probably associated with a primary phase, possibly related to the presence of volcanic glass, which was used as a temper in some recipes of CWA-PI pottery (Carosio and Ots 2022; Prieto Olavarría and Castro de Machuca 2017; Prieto Olavarría and Páez 2015). In firing experiments conducted on production pottery containing volcanic glass from Mount Vesuvius, primary analcime decomposed below 800 °C (Madrid, 2006). Therefore, the EFT for this individual should be estimated to be below 800 °C.

Excluding groups CGI04 and CGI06, each comprising only three individuals, a comparison of the larger groups suggests that the intended EFT could fall within the range of 850 °C to 950 °C, where the microstructure develops the extensive vitrification sintering stage, contributing to high mechanical strength (Kilikoglou et al. 1998; Tite et al. 2001). Most of the ceramics can be classified within this estimated EFT range, regardless of their type (*i.e.*, *urpu*, *ollas*, *pucos* or storage jars). However, the products from Uco Valley (CGI01) could consistently be fired at slightly lower temperatures.

Moreover, since all studied CWA-PI ceramics can be considered coarse pottery, adding aplastic inclusions (generally below 20%, as indicated by Carosio and Ots 2022) would imply a decrease in mechanical strength and an increase in toughness. These resultant performance characteristics would be adequate for storage and conveyance purposes, helping to prevent potential crack propagation and

vessel failure. These desirable attributes would be particularly important for storage jars and smaller fine vessels circulating within the region (*urpu*, *pucos* and *ollas*).

These performance characteristics were achieved using a coarse raw paste and high EFT, even though the limited firing control resulted in vessels with EFTs lower or higher than originally intended. This poor control could be related to the use of firing structures other than kilns, as revealed by the presence of the characteristic bloating pores microstructure that developed at higher temperatures in groups CGI02 (from Uspallata Valley), CGI05 (from the foothills of south San Juan province) and CGI06 (of unknown origin). This observation is lacking in group CGI01, either because firing temperatures were consistently lower or due to a lack of representation in the SEM subsample. Groups CGI03 and CGI04, of unknown origin, have not provided examples of fast heating, despite the presence of high-fired ceramics. Contrariwise, if the intended purpose of the pottery were for cooking, the performance characteristics would be enhanced by a low EFT with a microstructure of no vitrification sintering stage in order to arrest crack propagation produced by thermal shock.

The integrated results of this compositional and technological characterisation support local raw material procurement, simple technical skills, low intensity and scale of production, dispersed production *loci* and decentralised distribution. All these could be components of part-time production under elite or master potter control to meet a low but constant demand for valuables affiliated with Inca styles for political and symbolic purposes (Shortman and Urban 2004).

5. Conclusions

The archaeological study of CWA Provincial Inca pottery requires a holistic methodological approach that integrates all available material and social information. In this regard, this paper analyses low-visibility attributes through geochemical and mineralogical insights. Initially, it should be noted that the proposed analytical routine has enabled the recognition of meaningful ceramic groups and technical observations, shedding light on certain aspects of the organisation of production and distribution of Provincial Inca pottery, even though these conclusions should be regarded as hypotheses to be contrasted with further archaeological and archaeometric studies.

Six ceramic groups were identified through chemical characterisation, while 13 ceramics remained ungrouped. Three groups could be associated with the three areas under study (Uspallata and Uco Valleys and southern San Juan province), and only one is located within the space under Inca effective control (Uspallata Valley). As for the other three groups and ungrouped pottery, they could not be

assigned in this study to any probable provenance. Consequently, the organisation of Inca pottery production in CWA points towards a decentralised model with various production *loci* that share the same ceramic tradition. This model aligns with spatially dispersed small-scale societies of low social complexity and political centralisation, characteristics of the CWA context.

Despite the morphological diversity (such as *aryballos*, *storage jars*, *ollas*, *pucos*), the general technological attributes of CGI2 are similar to the pottery produced in Tambillos (Bárcena and Román 1990); that is, reddish compact pastes, fine granulometry, low density of inclusions (10-15%) and well-smoothed surfaces, sometimes also painted and polished. CGI1 has similar characteristics in appearance to CGI2 (morphology, colour, surface treatments), but the paste texture is more porous and the composition more heterogeneous in terms of temper frequency, size and distribution. However, the rest of the chemical groups have a more heterogeneous composition: CGI3 shows great variation in paste colour, density and texture. Pottery from Southern San Juan pastes displays higher density of temper, coarser grain size, and poorly sorted grain-size distribution, as well as smoothed, floated or puddled surfaces. CGI5 shares some technological similarities to CGI2, but combines Inca shapes, decorative techniques and patterns with local traditions (such as incised decoration, floated surfaces). Pastes are also more heterogeneous and denser than CGI2. Beyond the identified technological variability, the visible attributes are homogeneous within Inca canons, suggesting some degree of State control over demand and production.

The patterns observed point to intraregional interaction beyond the Inca effective control sector. The archaeometric characterisation could support the production in local settlements of Uco Valley and the foothills and plains of south San Juan province. Notably, the CWA Provincial Inca pottery from the latter area was not distributed in Uspallata Valley. In contrast, the pottery produced in Inca sites of Uspallata Valley was distributed to nearby sites in the same valley and the other two areas for sponsoring ceremonial hospitality or commensal practices.

Group CGI02 displays the highest homogeneity regarding technical and chemical characterisation and is particularly prevalent at Tambillos. Similarly, group CGI05 is especially present at RT285. According to the expectations about both sites as production centres, the results support that pottery produced in Uspallata Valley was most probably manufactured in Tambillos and had a widespread regional distribution. Conversely, the pottery produced in the foothills and plains of south San Juan province was probably produced in RT285, with its distribution mainly limited to the south San Juan area.

Chemical, mineralogical and microscopical characterisations, along with other studies of CWA Provincial Inca pottery, also contribute to characterising this technical tradition. The estimated firing temperature and microstructure of pottery denote a degree of control over firing conditions to produce vessels with high mechanical strength and toughness appropriate for storage and short-distance distribution purposes. According to archaeological studies in this region and other parts of *Tawantinsuyu*, *ollas* and *pucos* could have been used for cooking, but their most frequent use is found in funerary and State feasting contexts. *Urpú* and *pucos*, utilised in socio-political practices in south San Juan sites, came almost exclusively from Uspallata Valley through State distribution channels. In contrast, in Uco Valley, they are associated with group CGI01, whose origin is still unclear. Contrariwise, the *ollas* likely originated in other areas. Despite its big size, utilitarian pottery (storage jars) was mainly produced in Inca sites within Uspallata Valley, consumed locally and distributed regionally.

In CWA, Inca infrastructure and typical settlements support the argument of the Inca's effective control over Calingasta and Uspallata valleys, yet other processes concomitant to this domination extend regionally. Local communities were, to some extent, colonised, as the production and use of Inca-style ceramics under State sponsorship were imposed across the region. This stylistic influence lasted until European colonial times. Further archaeological and ethnohistorical data will have to be studied to identify the actors included in this process, likely including workers relocated to productive enclaves, whose political status, social roles and ethnic identities have yet to be determined.

References

Aitchison J (1986) *The statistical analysis of compositional data*. Monographs on statistics and applied probability. Chapman and Hall, London.

Aitchison J, Greenacre M (2002) Biplots of compositional data. *J R Stat Soc Ser C Appl Stat* 51: 375-392. <https://doi.org/10.1111/1467-9876.00275>

Alconini S (2013) El territorio Kallawaya y el taller alfarero de Milliraya: evaluación de la producción, distribución e intercambio interregional de la cerámica inka provincial. *Chungará* 45 (2): 277-292. <http://dx.doi.org/10.4067/S0717-73562013000200005>

Bárcena JR (1977) Informe sobre recientes investigaciones arqueológicas en el N. O. de la provincia de Mendoza, Argentina (Valle de Uspallata y zonas vecinas). (Con especial referencia al período incaico). *Actas del VII Congreso de Arqueología de Chile*, vol. II: 661-692. Kultrun, Santiago de Chile.

Bárcena JR (1998) El tambo real de Ranchillos. Mendoza, Argentina. *Xama* 6-11: 1-52.

Bárcena JR, Román A (1990 [1986-1987]) Funcionalidad diferencial de las estructuras del tambo de Tambillos: resultados de la excavación de los recintos 1 y 2 de la Unidad A del Sector III. *Anales de Arqueología y Etnología* XL-XLI: 7-81. <https://bdigital.uncu.edu.ar/16720>

Buxeda i Garrigós J (1999) Alteration and contamination of archaeological ceramics: the perturbation problem. *J Archaeol Sci* 26: 295-313. <https://doi.org/10.1006/jasc.1998.0390>

Buxeda i Garrigós J (2018) Compositional Data Analysis. In: López Varela, SL (ed). *The Encyclopedia of Archaeological Sciences*: 1-5. John Wiley and Sons, Oxford.

Buxeda i Garrigós J, Cau Ontiveros MA (1995) Identificación y significado de la calcita secundaria en cerámicas arqueológicas. *Complutum* 6: 293–309 <http://hdl.handle.net/2445/32743>

Buxeda i Garrigós J, Jones RE, Kilikoglou V, Levi ST, Maniatis Y, Mitchell J, Vagnetti L, Wardle KA, Andreou S (2003) Technology transfer at the periphery of the Mycenaean world: the cases of Mycenaean pottery found in central Macedonia (Greece) and the Plain of Sybaris (Italy), *Archaeometry* 45: 263-284. <https://doi.org/10.1111/1475-4754.00108>

Buxeda i Garrigós J, Kilikoglou V (2003) Total Variation as a Measure of Variability in Chemical Data Sets. In van Zelst L (ed) Patterns and Process. A Festschrift in Honor of Dr. Edward V Sayre: 185–198. Smithsonian Center for Materials Research and Education, Suitland.

Buxeda i Garrigós J, Madrid i Fernández M (2017) Designing Rigorous Research: Integrating Science and Archaeology. In W Hunt AM (ed.) The Oxford Handbook of Archaeological Ceramic Analysis: 19-47. Oxford University Press, Oxford. <https://doi.org/10.1093/oxfordhb/9780199681532.013.3>

Buxeda i Garrigós J, Mommsen H, Tsolakidou A (2002) Alterations of Na, K and Rb concentrations in Mycenaean pottery and a proposed explanation using x-ray diffraction. *Archaeometry* 44: 187-198. <https://doi.org/10.1111/1475-4754.t01-1-00052>

Buxeda i Garrigós J, Ots MJ, Madrid i Fernández M, Cahiza PA (2023) Inca provincial pottery of Central Western Argentina (CWA), <https://doi.org/10.34810/data791>, CORA.Repositori de Dades de Recerca, V1, UNF:6:LdNseJe5Wek+QISWwqtjUA== [fileUNF]

Cahiza P (2003) La dominación Inka en las tierras bajas de Mendoza y San Juan. Tesis doctoral. Facultad de Filosofía y Letras, UNCuyo, Mendoza (unpublished Ph.D).

Calderari M, Williams V (1991) Re-evaluación de los estilos cerámicos incaicos en el Noroeste Argentino. *Comechingonia* 7: 73-95.

Canals Frau S (1950) Exploraciones arqueológicas en el Antiguo Valle de Uco (Mendoza). Publicaciones XXII. Inst. de Arq., Lingüística y Folklore Dr. Pablo Cabrera. UN de Córdoba, Córdoba.

Carosio S, Ots MJ (2020) Prácticas de manufactura cerámica de las comunidades del Centro de Mendoza (Argentina) entre 1500 y 450 años AP. *Relaciones de la Sociedad Argentina de Antropología XLV*: 297-321. http://www.scielo.org.ar/scielo.php?script=sci_arttext&pid=S1852-14792020000200021&lng=es&ndrm=iso&dtlng=es

Carosio S, Ots MJ (2022) Pottery technology and provenance in southern Tawantinsuyu. A petrographic approach to Provincial Inca style. *Archaeol Anthropol Sci* 14:227. <https://doi.org/10.1007/s12520-022-01693-1>

Cau Ontiveros MA, Day PM, Montana G (2002) Secondary calcite in archaeological ceramics: Evaluation of alteration and contamination processes by thin section study. In Kilikoglou V, Y

Maniatis, A Hein (ed.) Modern trends in ancient ceramics: 9-18. BAR International Series 1011. Archaeopress, Oxford.

D'Altroy T, Earle T (1990) Staple finance, wealth finance and storage in the Inka political economy. *Curr Anthropol* 26: 187-206. <https://doi.org/10.1086/203249>

D'Altroy T, Lorandi AM, Williams V (1994) Producción y uso de cerámica en la economía política inca. In Shimada I (ed) *Tecnología y organización de la producción de cerámica prehispánica en Los Andes*: 395-441. Fondo Editorial de la Pontificia Universidad Católica del Perú, Lima.

Davenport J A (2020) The organisation of production for Inka Polychrome pottery from Pachacamac, Peru. *J Anthropol Archaeol* 60: 101235. <https://doi.org/10.1016/j.jaa.2020.101235>

De la Fuente G, Ferguson JR, Glascock M (2015) Chemical and petrographic analysis of pre-hispanic pottery from the Southern Abaucán Valley, Catamarca, Argentina. *Archaeometry* 57: 1-17. <https://doi.org/10.1111/arcm.12081>

Egozcue JJ, Pawlowsky-Glahn V (2011) Basic Concepts and Procedures. In Pawlowsky-Glahn V, A Buccianti (ed) *Compositional Data Analysis. Theory and Applications*: 12-28. Wiley, Chichester. <https://doi.org/10.1002/9781119976462.ch2>

Fabbri B, Gualtieri S, Shoval S (2014) The presence of calcite in archaeological ceramics. *J Eur Ceram Soc* 34 (7): 1899-1911. <https://doi.org/10.1016/j.jeurceramsoc.2014.01.007>

García A. 1996. La dominación inca en el Centro Oeste argentino y su relación con el origen y la cronología del registro Viluco. *Anales de Arqueología y Etnología* 48/49: 57-72.

Greenacre M (2010) Biplots in practice. BBVA Foundation Manuals. Fundación BBVA, Bilbao. https://www.fbbva.es/wp-content/uploads/2017/05/dat/DE_2010_biplots_in_practice.pdf

Hayashida FM (1999) Style, Technology, and State Production: Inka Pottery Manufacture in the Leche Valley, Peru. *Lat Am Antiq* 10 (4): 337-352. <https://doi.org/10.2307/971961>

Heimann RB, Maggetti M (2014) *Ancient and Historical Ceramics. Materials, Technology, Art, and Culinary Traditions*. Schweizerbart Science Publishers, Stuttgart.

Jafarzadeh AA, Burnham CP (1992) Gypsum crystals in soils. *Eur J Soil Sci* 43: 409-420. <https://doi.org/10.1111/j.1365-2389.1992.tb00147.x>

Kilikoglou V, Vekinis G, Maniatis Y, Day PM (1998) Mechanical performance of quartz-tempered ceramics: part I, strength and toughness. *Archaeometry* 40(2): 261-279. <https://doi.org/10.1111/j.1475-4754.1998.tb00837.x>

Lagiglia H (1978) La cultura de Viluco del Centro Oeste Argentino. *Revista del Museo de Historia Natural de San Rafael* III (1-4): 227-265.

Madrid i Fernández M (2006) Estudi arqueològic i caracterització arqueomètrica de la "terra sigillata" de la ciutat de Baetulo (Badalona). Tesis doctorals electròniques, Universitat de Barcelona, Barcelona. Retrieved January 16, 2017, from <http://www.tdx.cat/handle/10803/2591>.

Maggetti M (1981) Composition of Roman pottery from Lousonna (Switzerland). In Hughes MJ (ed) *Scientific studies in ancient ceramics*: 33-49. British Museum Occasional Paper 19, London.

Maggetti M (1982) Phase analysis and its significance for technology and origin. In Olin JS, AD Franklin (ed.). *Archaeological Ceramics*: 121-133. Smithsonian Institution Press, Washington D.C.

Magurran A E (2004) *Measuring Biological Diversity*, Blackwell Science Ltd., Oxford.

Maniatis Y, Simopoulos A, Kostikas A (1981) Moessbauer Study of the Effect of Calcium Content on Iron Oxide Transformations in Fired Clays. *J Am Ceram Soc* 64(5): 263-269. <https://doi.org/10.1111/j.1151-2916.1981.tb09599.x>

Maniatis Y, Simopoulos A, Kostikas A, Perdikatsis V (1983) Effect of reducing atmospheres on minerals and iron oxides developed in fired clays: the role of Ca. *J Am Ceram Soc* 66(11): 773-781. <https://doi.org/10.1111/j.1151-2916.1983.tb10561.x>

Maniatis Y, Tite MS (1975) A Scanning Electron Examination of the Bloating of Fired Clays, *Transactions and Journal of the British Ceramic Society* 74: 229-32.

Maniatis Y, Tite MS (1978) Ceramic technology in the Aegean World during the Bronze Age. In Dumas C (ed). *Thera and the Aegean World I. Papers presented at the Second International Scientific Congress, Santorini, Greece, August 1978*: 483-492. London.

Maniatis Y, Tite MS (1981) Technological Examination of Neolithic-Bronze Age Pottery from Central and Southeast Europe and from the Near East. *J Archaeol Sci* 8: 59-76. [https://doi.org/10.1016/0305-4403\(81\)90012-1](https://doi.org/10.1016/0305-4403(81)90012-1)

Maniatis Y, Tsirtsoni Z (2002) Characterisation of a black residue in a decorated Neolithic pot from Dikili Tash, Greece: an unexpected result. *Archaeometry* 44(2): 229-239. <https://doi.org/10.1111/1475-4754.t01-1-00055>

Manning CD, Raghavan P, Schütze H (2008) *Introduction to Information Retrieval*, Cambridge University Press, Cambridge. <https://doi.org/10.1017/CBO9780511809071>

Martín-Fernández JA, Buxeda i Garrigós J, Pawlowsky-Glahn V (2015) Logratio Analysis in Archeometry: Principles and Methods. In Barceló JA, I Bogdanovic (ed). *Mathematics and Archaeology*: 178-189. Science Publishers, Boca Raton. <https://doi.org/10.1201/b18530>

Murra J (2002 [1978]) Los olleros del Inca. Hacia una historia y arqueología del Qollasuyo. In Murra J *El Mundo Andino: población, medio ambiente y economía*: 287-293. IEP, PUC, Lima.

Ots MJ (2008) Aportes del Análisis Petrográfico de Cortes Delgados para la Caracterización y Clasificación del Estilo Cerámico Viluco Inca. *Boletín del Laboratorio de Petrología y Conservación cerámica* 1(2): 12-21. <https://arqueologia.unca.edu.ar/assets/boletin-lpcc-vol1-n2-a1.pdf>

Ots MJ, Cahiza P (2013) Caracterización de la frontera suroriental del Tawantinsuyu (Sur de San Juan – Norte y Centro de Mendoza, siglos XV-XVI). In Gascón M, MJ Ots (ed). *Periferias y Fronteras en la Arqueología y la Historia*: 30-62. Dunken, Buenos Aires.

Ots MJ, Cahiza P (2016) Archaeometric approaches to the functionality of combustion structures (CS) from Central Western Argentina. In de la Fuente G, E Stovel (ed). *Vessels explored: Applying Archaeometry to South American Ceramics and their Production*: 77-87. *British Archaeological Reports (BAR-IS)* 2808. Archaeopress, Oxford.

Picon M (1973) *Introduction à l'étude technique des céramiques sigillées de Lezoux*. Centre de recherches sur les techniques gréco-romaines 2. Faculté des Sciences Humaines, Dijon.

Prieto Olavarría C (2012) La producción y función de la cerámica indígena durante la dominación incaica y la colonia en Mendoza (Argentina). *Intersecciones en Antropología* 13: 71-87. http://www.scielo.org.ar/scielo.php?script=sci_abstractandpid=S1850-373X2012000100005

Prieto Olavarría C, Castro de Machuca B (2017) Petrographic characterisation and identification of temper sources in local ceramics during the Inca domination and early Spanish colony (Mendoza, west-central Argentina). *J Archaeol Sci Rep* 13: 351-360. <https://doi.org/10.1016/j.jasrep.2017.04.011>

Prieto Olavarría C, Páez MC (2015) Presencia de inclusiones piroclásticas en la cerámica de los siglos XV a XVII en el Centro Oeste y Noroeste argentino. *Chungara* 47: 441-453. <http://dx.doi.org/10.4067/S0717-73562015005000043>

Prieto Olavarría C, Tobar V (2017) Interacciones y lenguajes visuales en la cerámica local de los períodos Inca y colonial (centro oeste argentino). *Estudios atacameños* 55: 135-151. <http://dx.doi.org/10.4067/S0718-10432017005000018>

R Core Team (2021) *R: A language and environment for statistical computing*. R Foundation for Statistical Computing, Vienna, Austria. <https://www.R-project.org/> Accessed October 1st 2022.

Rice P (2009) Late Classic Maya Pottery Production: Review and Synthesis. *J Archaeol Method Theory* 16:117–156. <https://www.jstor.org/stable/25653117>

Roberts JP (1963) Determination of the firing temperature of ancient ceramics by measurement of thermal expansion. *Archaeometry* 6: 21-25. <https://doi.org/10.1111/j.1475-4754.1963.tb00574.x>

Rodríguez-Navarro C, Ruíz-Agudo E, Luque A, Rodríguez-Navarro AB, Ortega-Huertas M (2009) Thermal decomposition of calcite: mechanisms of formation and textural evolution of CaO nanocrystals. *Am Mineral* 94: 578-593. <https://doi.org/10.2138/am.2009.3021>

Schwedt A, Mommsen H, Zacharias N, Buxeda i Garrigós J (2006) Analcime crystallisation and compositional profiles – comparing approaches to detect post-depositional alterations in archaeological pottery. *Archaeometry* 48: 237-251. <https://doi.org/10.1111/j.1475-4754.2006.00254.x>

Shannon CE (1948) A Mathematical Theory of Communication. *The Bell System Technical Journal* 27: 379–423, 623–656. <https://doi.org/10.1002/j.1538-7305.1948.tb01338.x>

Shortman EM, PA Urban (2004) Modeling the Roles of Craft Production in Ancient Political Economies. *Journal of Archaeological Research* 12(2): 185-226. <https://doi.org/10.1023/B:JARE.0000023712.34302.49>

Sneath PHA, Sokal RR (1973) *Numerical taxonomy. The principles and practice of numerical classification*, W. H. Freeman and Company, San Francisco.

Terraza V, Bárcena JR (2016) Los estilos tecnológicos cerámicos de La Chanchería como indicadores de modos de hacer y de producir de las sociedades tardías del valle de Uspallata (NO de Mendoza). *Revista del Museo de Antropología, Suplemento especial 1*: 129-136.

Tite MS, Kilikoglou V, Vekinis G (2001) Strength, toughness and thermal shock resistance of ancient ceramics, and their influence of technological choice. *Archaeometry* 43(3): 301-324. <https://doi.org/10.1111/1475-4754.00019>

Tite MS, Maniatis Y, Meeks ND, Bimson M, Hughes MJ, Leppard SC (1982) Technological Studies of Ancient Ceramics from the Near East, Aegean and Southeast Europe. In Wertime TA, SF Wertime (ed). *The evolution of the first fire-using industries*: 61-71. Smithsonian Institution Press, Washington.

Tsantini E, Buxeda i Garrigós J, Cau Ontiveros MA, Orfila Pons M (2004) Caracterización arqueométrica de la cerámica común producida en la villa romana de Sa Mesquida (Mallorca). *Pyrenae* 35: 157-186. <https://raco.cat/index.php/Pyrenae/article/view/145121>

Tuñón López JA, Sánchez Vizcaíno A, Chiavazza H, Montejo Gámez M (2012) Los colores de la cerámica Viluco y Diaguita chilena: determinación de pigmentos utilizados en la decoración cerámica indígena del norte de Mendoza (Argentina) mediante microespectroscopía Raman y microfluorescencia de energía dispersiva de rayos X. *Estudios Arqueológicos de Oeiras* 19: 193-202.

van de Boogaart KG, Tolosana-Delgado R (2013) *Analysing Compositional Data with R*. Springer-Verlag, Berlin Heidelberg.

Whitney DL, Evans BW (2010) Abbreviations for names of rock-forming minerals. *Am Mineral* 95: 185-187. <https://doi.org/10.2138/am.2010.3371>

Yu QL, Brouwers HJH (2012) Thermal properties and microstructure of gypsum board and its dehydration products: A theoretical and experimental investigation. *Fire Mater* 36: 575-589. <https://doi.org/10.1002/fam.1117>

Zhang Q, Kasai E, Saito F (1996) Mechanochemical changes in gypsum when dry ground with hydrated minerals. *Powder Technol* 87: 67-71. [https://doi.org/10.1016/0032-5910\(95\)03069-7](https://doi.org/10.1016/0032-5910(95)03069-7)

Supplementary materials

Small-scale pottery production and distribution in the southern confines of the Inca empire. An archaeometric insight to define the Provincial style.

ARCHAEOLOGICAL AND ANTHROPOLOGICAL SCIENCES

M. J. Ots*, J. Buxeda i Garrigós, M. Madrid i Fernández, P. A. Cahiza

*Corresponding author. Consejo Nacional de Investigaciones Científicas y Técnicas, Instituto Nacional de Ciencias Humanas, Sociales y Ambientales / Universidad Nacional de Cuyo, Facultad de Filosofía y Letras, Instituto de Arqueología y Etnología. Mendoza-Rca (Argentina). mjots@mendoza-conicet.gob.ar

Site	Geographical Coordinates	Location	Reference
Agua Amarga	S33°28'18.5'' W69°11'29.3''	Archaeological site	Ots, 2007
Atamisque	S33°16'42.17'' W69°10'12.62''	Modern village	Google earth
Potrero Chanchería	S32°34'47.21'' W69°21'21.56''	Archaeological site	Terraza, Bárcena 2016
Tambillos	S32°23'03.03'' W69°23'28.58''	Archaeological site	Google earth
Ciénaga de Yalguaraz	S32°07'56.84'' W69°19'54.12''	Locality	Google earth
Ranchillos	S32°36'21.79'' W69°28'06.48''	Archaeological site	Google earth
Tambillitos	S32°44'52.46'' W69°34'46.64''	Archaeological site	Google earth
Altos de Melián	S32°10'26.0'' W68°16'20.5''	Archaeological site	Cahiza 2003
RT 285	S32°05'38.2'' W68°36'36.9''	Archaeological site	Cahiza 2003
El Pozo	S32°05'12.5'' W68°38'33.8''	Archaeological site	Cahiza 2003
A° Cieneguita	S32°04'32.0'' W68°39'37.7''	Archaeological site	Cahiza 2003
Retamito	S32° 6' 13'' W68°35'53''	Archaeological site	Cahiza 2003

Geographical coordinates (DMS) of the sites mentioned in the text